

Phase separation and near-critical fluctuations in two-component lipid membranes: Monte Carlo simulations on experimentally relevant scales

Jens Ehrig, Eugene P Petrov and Petra Schwille

Biophysics, BIOTEC, Technische Universität Dresden, Tatzberg 47/49, 01307 Dresden, Germany

E-mail: petrov@biotec.tu-dresden.de

Abstract. By means of lattice-based Monte Carlo simulations, we address properties of two-component lipid membranes on the experimentally relevant spatial scales of order of a micrometer and time intervals of order of a second, using DMPC/DSPC lipid mixtures as a model system. Our large-scale simulations allowed us to obtain important results previously not reported in simulation studies of lipid membranes. We find that, within a certain range of lipid compositions, the phase transition from the fluid phase to the fluid–gel phase coexistence proceeds via near-critical fluctuations, while for other lipid compositions this phase transition has a quasi-abrupt character. The line tension characterizing lipid domains in the fluid–gel coexistence region is found to be ≈ 2 pN. When approaching the critical point, the line tension, the inverse correlation length of fluid–gel spatial fluctuations, and the corresponding inverse order parameter susceptibility of the membrane vanish. All these results are in agreement with recent experimental findings for model lipid membranes. We observe transient subdiffusive behaviour of lipids in the presence of near-critical fluctuations, which is a new result important for understanding the origins of subdiffusion in cell membranes. Our analysis of the domain coarsening dynamics after an abrupt quench of the membrane to the fluid–gel coexistence region reveals that lateral diffusion of lipids plays an important role in the fluid–gel phase separation process.

PACS numbers: 87.14.Cc, 87.15.ak, 87.16.dj, 87.16.dt

Keywords: Monte Carlo simulation; lipid membrane; DMPC; DSPC; phase diagram; critical fluctuations; anomalous diffusion; dynamic scaling; line tension

1. Introduction

The membrane plays a very important role in the cell, not only by defining its boundaries and boundaries of the cell organelles, but also by taking an active part in cell functioning, as many key processes take place in or across the cell membrane. The plasma membrane is a very complex system comprised of lipids, polysaccharides, and proteins, all strongly interacting with each other. These lipid–lipid and lipid–protein interactions induce the lateral microheterogeneity of the cell membrane, which is believed to be crucial in providing its high functionality [1]. The idea of the function-related lateral microheterogeneity of the membrane was formulated in a compact form by Simons and Ikonen [2] in the form of the concept of lipid rafts. The original concept of lipid rafts involved the dynamic clustering of sphingolipids and cholesterol, supposedly forming moving platforms in the cell membrane to which certain proteins would attach [2]. Presently, the understanding is that the interaction of lipids with membrane proteins and the cytoskeleton, as well as effects of local curvature, play an important role in organization of the lateral microheterogeneity of the cell membrane [3, 4, 5, 6]. Consequently, the term membrane rafts appears to be more appropriate [7].

In spite of the importance of lipid–protein interactions, the behaviour of the lipid component of the cell membrane is still believed to govern its properties to a large extent. In agreement with that, it was found that studies of model membrane systems – both *in vitro* [8] and *in silico*, i.e., via numerical simulations [9, 10, 11, 12] – give valuable information on the lateral organization and dynamics of lipid molecules, which provides a deeper insight into the structure and function of plasma membranes.

Numerical simulations are an extremely fruitful approach to membrane studies, giving access to information which is either difficult or even impossible to access using present-day experimental techniques. Depending on particular aims and goals, a wide arsenal of simulation techniques has been developed to study model membrane systems. A particular choice of the simulation approach largely depends on the amount of the fine molecular details, as well as spatial scales and time ranges of relevance for a particular problem addressed by a researcher. Broadly, the approaches to numerical simulations of lipid membranes include molecular dynamics methods and their coarse-grained versions, mean-field based continuum model simulations, and lattice-based methods.

Molecular dynamics simulations provide the most detailed approach to describe the structure and dynamics of membranes. They employ an atomistic description of the lipid membrane and thus, with the presently available computational resources, are able to cover spatial scales up to a few nm and time scales of $\leq 1 \mu\text{s}$ [13, 14]. By using coarse-grained molecular dynamics simulations which sacrifice the very fine atomistic details for the sake of a better computational efficiency [9, 12, 15] these scales can be extended to $\approx 100 \text{ nm}$ and $\approx 10 \mu\text{s}$. Further coarse-graining [16, 17], by representing a cluster of a few ten lipid molecules as one particle, allows for simulations of membranes consisting of ~ 6000 coarse-grained particles, which is equivalent to the total number of ~ 60000 lipid molecules in a simulated membrane. On the other hand, this type

of coarse-graining does not allow one to address diffusional motion of individual lipid molecules in the membrane.

Mean field-based continuum simulations of the lipid membrane organization can be made more realistic by using lipid interaction parameters and lipid chain order parameter libraries extracted from molecular dynamics simulations [18]. For ternary lipid membrane systems, these simulations can currently address spatial scales of a few tens of nm [18]. In view of the continuum character of the model, they do not, however, provide information on the lateral diffusion of membrane components.

Continuum simulations [19, 20], based on solving evolution equations for a compositional or phase field, are primarily concerned with the issue of the phase separation behaviour of lipid membranes [21, 22, 23]. These simulations address much larger spatial scales of order of a few hundred nm. On the other hand, this approach does not seem to be able to reproduce the complete phase diagram of a real lipid mixture. Additionally, these simulations do not provide information on lateral diffusion in the membrane.

Lattice-based Monte Carlo simulations constitute the computationally least demanding way to numerical modelling of lipid membranes. Not surprisingly, first lattice-based simulations of the single-component lipid membrane date back to the early 1980s [24]. Later, this approach based on either ten-state Potts model or Ising-like models was successfully used to study phase transitions in one- and two-component lipid membranes, as well as the effects of lipid-protein and lipid-drug interactions on the phase separation in lipid membranes (see, e.g., [25, 26, 27, 28, 29, 30]). Although these lattice-based approaches do not even attempt at reproducing the membrane structure and dynamics in full detail on the atomic and molecular scale, they provide a surprisingly realistic description of the phase separation and dynamics in lipid membranes. Additionally, because of the simplified description of the membrane, lattice-based simulations are capable of describing the membrane behaviour on much larger spatial scales and substantially longer time intervals than the above-mentioned atomistic and coarse-grained simulations with the same computational expenses. While the previously published lattice-based simulations addressed one- or two-component lipid membranes on spatial scales from ten to hundred nm, the recent rapid progress in computer hardware presently allows one to substantially expand the spatial scales and time intervals addressed in lattice-based simulations.

The aim of the present study is to address the properties of model lipid membranes using a reasonably simple, but still realistic enough, model on the experimentally relevant spatial scales of order of a micrometer and time scales of order of a second. Simulations on these spatial scales and time intervals should provide results which can be directly compared with experimental results obtained using optical microscopy-based methods routinely used in membrane studies. Our goal was, therefore, to develop a lattice-based Monte Carlo simulation approach that would not only provide an adequate description of the membrane phase behaviour and membrane dynamics, but in addition would be computationally efficient in order to reach the required spatial and temporal

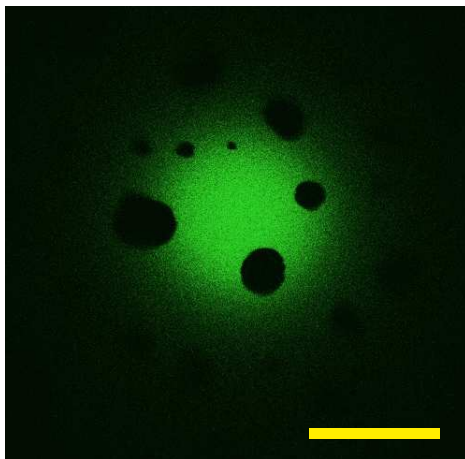


Figure 1. Confocal fluorescence microscopy image of the upper pole of a giant unilamellar vesicle (DMPC/DSPC 50/50) exhibiting fluid–gel phase separation. Gel-phase domains, which coarsen and coalesce with time, appear on the image as dark areas. Scale bar: 20 μm .

scales.

We chose to study membranes consisting of a binary mixture of DMPC (1,2-dimyristoyl-*sn*-glycero-3-phosphocholine, $T_m = 297$ K) and DSPC (1,2-distearoyl-*sn*-glycero-3-phosphocholine, $T_m = 328$ K), which for a range of lipid compositions and temperatures shows coexistence of fluid and gel phases (figure 1). The phase diagram of this system has been extensively studied experimentally (see, e.g., [29, 30, 31, 32, 33, 34, 35, 36, 37]). Some aspects of the phase behaviour of the same lipid mixture have been previously addressed in a series of lattice-based Monte Carlo simulations (see, e.g., [29, 30, 37]). Therefore, the choice of the well-studied DMPC/DSPC lipid systems as an object of our study allowed for a direct comparison of the results of our numerical simulations with experimental data, as well as with results obtained in simulation studies of the same lipid system carried out by other groups.

In the present paper, the main emphasis is on the phase diagram of the DMPC/DSPC lipid system, including the near-critical behaviour of the membrane close to its critical point, as well as the properties of membrane domains, including the line tension of the phase interface, and domain growth kinetics. We also address the aspects of lateral diffusion in the membrane, albeit only briefly (a study focused on the effects of near-critical fluctuations in a two-component membrane and the effects of cytoskeleton will be published elsewhere [38]).

2. Materials and Methods

2.1. Experimental

The lipids 1,2-dimyristoyl-*sn*-glycero-3-phosphocholine (DMPC), 1,2-distearoyl-*sn*-glycero-3-phosphocholine (DSPC) and the fluorescent lipid marker 1,2-dipalmitoyl-*sn*-

glycero-3-phosphoethanolamine-N-(lissamine rhodamine B sulfonyl) (N-Rhod-DPPE) were purchased from Avanti Polar Lipids (Alabaster, AL), diluted in a chloroform-methanol (2:1) mixture, aliquoted, and stored at -20°C in argon atmosphere. Giant unilamellar vesicles (GUVs) were prepared by electroformation on a platinum wire [39]. Multilamellar vesicle suspensions were obtained from rehydration of a dry lipid film. Differential scanning calorimetry (DSC) experiments were performed on a VP-DSC calorimeter (MicroCal, Northampton, MA) with a scan rate of $2 - 3 \text{ K/h}$ and a medium (“mid”) feedback.

The temperatures of the onset and completion of the phase transition were determined from experimentally measured excess heat capacity curves using an empirical approach known as the tangent method. To do that, a tangential line is drawn to a heat capacity curve at its low-temperature (onset of the phase transition) or high-temperature (completion of the phase transition) slopes, and the respective temperature is determined as the zero-crossing point of this tangential line. Plotting the temperatures of the onset and completion of the phase transition as a function of the composition of the lipid mixture allows one to construct an empirical experimental phase diagram of the lipid mixture.

2.2. Monte Carlo Simulations

To achieve a higher computational efficiency in Monte Carlo simulations of membrane dynamics on the experimentally relevant spatial scales (of order of a micrometer) and time intervals (of order of a second), where a particular type of lipid packing and fine molecular details should be of little importance, we make one more step toward simplification of the description within the framework of the membrane lattice model. To represent a membrane, instead of a triangular lattice of lipid chains [29, 30], we use a *square* lattice of lipid *molecules* (figure 2). In this representation, neither the orientation of a lipid molecule within the membrane plane nor the states of individual lipid chains of the lipid molecule has to be accounted for. The model assumes that each of the lipid molecules placed on a square lattice with periodic boundary conditions can exist in either gel or fluid state, and can move laterally via next-neighbour exchange. Formally, this model is an Ising model with a conserved order parameter (representing lipids) decorated by an Ising model with a non-conserved order parameter (representing lipid states).

The fundamental step of the MC simulation consists of two sub-steps. In the first sub-step, an attempt is made to change the state of a randomly chosen lipid (from gel to fluid or vice versa). The second sub-step is an attempt to exchange the positions of a randomly chosen pair of next neighbours on the lattice.

For each sub-step the change in the Gibbs free energy

$$\begin{aligned} \Delta G = & \Delta N_1^{\text{F}} (\Delta E_1 - T \Delta S_1) + \Delta N_2^{\text{F}} (\Delta E_2 - T \Delta S_2) + \Delta N_{11}^{\text{GF}} w_{11}^{\text{GF}} \\ & + \Delta N_{22}^{\text{GF}} w_{22}^{\text{GF}} + \Delta N_{12}^{\text{GG}} w_{12}^{\text{GG}} + \Delta N_{12}^{\text{FF}} w_{12}^{\text{FF}} + \Delta N_{12}^{\text{GF}} w_{12}^{\text{GF}} + \Delta N_{21}^{\text{GF}} w_{21}^{\text{GF}}, \end{aligned} \quad (1)$$

is calculated. Here, ΔE_i and ΔS_i are the changes in the internal energy and entropy of

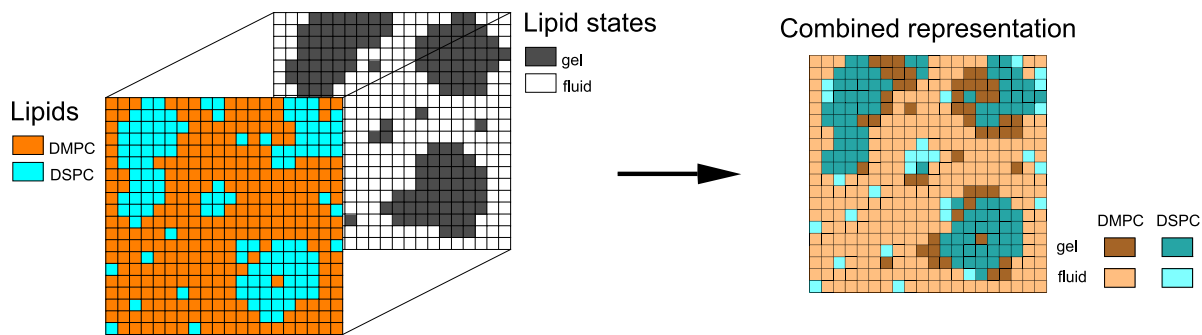


Figure 2. Square lattice model used in this work to simulate lipid membranes consisting of a mixture of two lipids (DMPC and DSPC in the present study). Individual lipid molecules occupy the nodes of a square lattice. Each of the two lipids (orange, cyan) can exist in either gel or fluid conformational state (black, white). The combined representation via four-colour coding makes it possible to see the complete configuration of the lattice in a single snapshot.

a molecule of lipid i when it switches its state from gel to fluid, and w_{ij}^{mn} are the next-neighbour interaction parameters of lipids i and j being in states n and m , respectively. In the simulation, the attempts of the state change and next-neighbour exchange are accepted with probability $p = 1$ for $\Delta G < 0$ and $p = \exp(-\Delta G/RT)$ for $\Delta G \geq 0$.

For an $L \times L$ lattice, one MC cycle consists of a chain of L^2 elementary MC steps. After each cycle, the enthalpy of the lattice is calculated as follows: $H = N_1^F \Delta E_1 + N_2^F \Delta E_2 + N_{11}^{GF} w_{11}^{GF} + N_{22}^{GF} w_{22}^{GF} + N_{12}^{GG} w_{12}^{GG} + N_{12}^{FF} w_{12}^{FF} + N_{12}^{GF} w_{12}^{GF} + N_{21}^{GF} w_{21}^{GF}$.

MC simulations naturally give access to a number of thermodynamic parameters of the system. For example, the excess heat capacity $C(T)$ can be calculated from the variance of equilibrium fluctuations of the total lattice enthalpy H as follows: $C(T) = \langle (H - \langle H \rangle)^2 \rangle / RT^2$.

To adjust the lipid interaction parameters, we used the approach previously described by Sugár *et al.* [27, 29]: temperature-dependent excess heat capacity curves were obtained from MC simulations for a range of membrane compositions and compared with experimentally measured heat capacity curves, and the parameters w_{ij}^{mn} were varied until a reasonable agreement with experimental DSC data was achieved. Since a simpler lattice representation of the lipid system (lipid molecules arranged on a square lattice) was used in our simulations compared to the previous studies [29, 30] (lipids represented as dimers of acyl chains arranged on a triangular lattice), the lipid interaction parameters w_{ij}^{mn} in our study differ from those used in previous publications [29, 30] (table 1).

For each of the membrane compositions and temperatures addressed in the present study, simulation started with a random initial configuration of the membrane where lipids were randomly distributed on the lattice and all assigned to be in the fluid state (i.e., configurations corresponding to an infinitely high temperature). After that, the system was abruptly quenched to a particular target temperature, and simulations were carried out while keeping the temperature constant. The whole time-dependent

Table 1. Thermodynamic parameters of lattice-based MC simulations of the DMPC/DSPC lipid membranes used in the present work and previous publications [29, 30].^a

MC study	Thermodynamic Parameters									
	ΔE_1 (Jmol ⁻¹)	ΔE_2 (Jmol ⁻¹)	ΔS_1 (Jmol ⁻¹ K ⁻¹)	ΔS_2 (Jmol ⁻¹ K ⁻¹)	w_{11}^{GF} (Jmol ⁻¹)	w_{22}^{GF} (Jmol ⁻¹)	w_{12}^{GF} (Jmol ⁻¹)	w_{21}^{GF} (Jmol ⁻¹)	w_{12}^{GG} (Jmol ⁻¹)	w_{12}^{FF} (Jmol ⁻¹)
Ref. [29], triangular lattice of lipid chains	12699.2	21966	42.651	67.015	1353.31	1474.11	1548.08	1715.44	564.84	334.72
Ref. [30], triangular lattice of lipid chains	13165	25370	44.31	77.36	1353	1474	1548	1716	607	251
Present work, square lattice of lipids	26330	50740	88.653	154.695	1827	1622	4025	4460	1412	502

^a Simulations by Sugár *et al.* [29] and Hac *et al.* [30] were carried out on the triangular lattice of lipid chains. The parameters used in the present work differ from those of [29, 30] due to the fact that simulations were carried out on a square lattice of lipid molecules.

evolution of the membrane starting with the abrupt temperature quench was recorded to study the domain coarsening and growth dynamics. To calculate the excess heat capacities and correctly address the other stationary properties of the membrane, including lipid diffusion dynamics, line tension of lipid domains, correlation lengths and susceptibilities, the membrane was first equilibrated. To ensure that the system has reached the full equilibrium, we verified whether the mean total lattice enthalpy relaxed to a constant value. In cases where equilibrium membrane configurations within the fluid–gel phase coexistence region of the phase diagram were required, the complete equilibration was additionally checked by visual inspection of membrane snapshots.

To represent the translational motion dynamics of lipids in the fluid and gel states in a realistic way, a rate function controlling the likelihood of next-neighbour exchange depending on the number of gel neighbours was introduced, as suggested in [30], to ensure a lower mobility of lipids in the gel environment. In particular, for two neighbouring lipids the next-neighbour exchange is accepted with a probability $r = \exp[-(N_{\text{gel neighbours}}/N_{\text{neighbours}})(\Delta E/k_{\text{B}}T)]$, where $N_{\text{neighbours}}$ ($N_{\text{gel neighbours}}$) is the number of the next neighbours (in the gel state) for the pair of lipids attempting to exchange their positions; in our simulations on the square lattice of lipids $N_{\text{neighbours}} = 6$. The quantity $\Delta E \geq 0$ corresponds to the activation energy barrier for the next-neighbour exchange in the all-gel environment compared to the all-fluid environment. In our simulations, ΔE was adjusted to provide ca. 40 times slower translational diffusion of lipids in the gel phase compared to the fluid phase. Since the transition probability between the gel and fluid conformations of the lipid molecule in our simulations depends only on its immediate environment, and does not involve any time delay, it follows that

at least the equilibrium properties of the membrane should not depend on the rate function.

Simulations were typically carried out on 600×600 or 400×400 lattices, which corresponds to a membrane patch consisting of 3.6×10^5 and 1.6×10^5 lipid molecules, respectively. MC simulations were run for up to 2×10^7 MC cycles, which allowed us to collect the necessary data for the analysis of thermodynamic properties of the membrane and translational diffusion of lipid molecules.

The spatial scale and time intervals addressed in our simulations can be obtained by relating the simulation lattice size to the lipid head group dimensions, and subsequently finding the MC step duration by relating translational diffusion of lipids to experimental data. By assuming the lipid head group having a size of ca. $0.8 \times 0.8 \text{ nm}^2$ and using experimental data on DMPC diffusion coefficient in the fluid phase [40], we find that one MC cycle of our simulations corresponds to $\approx 50 \text{ ns}$. Thus, our simulations describe the behaviour of a membrane fragment of a size of $\approx 0.48 \times 0.48 \mu\text{m}^2$ over time intervals of $\approx 1 \text{ s}$. These are indeed the experimentally relevant scales we planned to achieve in our simulations.

The program code is fully original and is written in Fortran completely from scratch except for the random number generation routine. The use of a good pseudo-random number generator is essential for the success of a Monte Carlo simulation study. In our simulations we therefore used the Mersenne Twister routine [41] providing sequences of pseudo-random numbers equidistributed in 623 dimensions characterized by an extremely long period of $2^{19937} - 1 \approx 4.3 \times 10^{6001}$. The Compaq Visual Fortran Compiler Ver. 6.6a (Compaq Computer Corporation, Houston, TX) was used for compilation. Simulation results were analyzed using original dedicated routines written in MATLAB Ver. R2007b (The MathWorks, Natick, MA) and Fortran.

Monte Carlo simulations were carried out on a workstation (Intel Core2 Quad Extreme CPU X9770 3.2 GHz, 4 GB RAM) running under Windows XP. Under these conditions, a simulation run on a 600×600 lattice for 2×10^7 MC cycles takes about 700 h of CPU time. The simulation method very naturally offers the opportunity of parallel implementation, which can further substantially speed-up the computation. Recent advances in the use of GPU-based computations [42, 43] also offer impressive speed-up of lattice based simulations and are planned to be implemented in our future work.

2.3. Data Analysis

2.3.1. Analysis of membrane configurations. To analyze the spatial distributions of lipids and lipid states, the radial autocorrelation function $G(r)$ and the circularly averaged structure function $S(k)$ were calculated from the radial distribution function $g(r)$ as follows [44, 45, 46]

$$G(r) = g(r) - 1, \quad (2)$$

$$g(r) = \bar{\rho}^{-2} \left\langle \sum_i \sum_{j \neq i} \delta(\mathbf{r}_i) \delta(\mathbf{r}_j - \mathbf{r}) \right\rangle, \quad (3)$$

$$S(k) = 1 + \bar{\rho} \mathcal{F} \{G(r)\}, \quad (4)$$

where $\rho(\mathbf{r})$ is the local particle density and $\bar{\rho}$ is the spatially averaged particle density. The fact that the particles cannot take arbitrary positions but rather occupy sites on the square lattice is taken into account to avoid artifacts in spatial and angular averaging. When studying equilibrium membrane properties, structure functions $S(k)$ were averaged over several hundred equilibrium configurations of the membrane at a given temperature and composition.

2.3.2. Analysis of lipid diffusion and simulation of FCS experiments. To study the lateral diffusion of lipid molecules, positions (x, y) of a small fraction ($< 0.05\%$) of lipid molecules were recorded, and the time- and ensemble-averaged mean-square displacement $MSD(\tau)$ was calculated

$$MSD(\tau) = \frac{1}{t_{\max} - \tau} \sum_{t=1}^{t_{\max} - \tau} \{[x(t) - x(t + \tau)]^2 + [y(t) - y(t + \tau)]^2\}, \quad (5)$$

where τ , t , and t_{\max} are integers giving time in units of MC cycles; here, τ denotes the time lag, and t_{\max} is the total length of the lipid molecule trajectory.

Additionally, fluorescence correlation spectroscopy (FCS) [47] measurements were simulated: the tracked particles were assumed to be fluorescent, and the autocorrelation function $G(\tau) = \langle \delta F(t) \delta F(t + \tau) \rangle / \langle F \rangle^2$ of fluorescence intensity fluctuations $\delta F(t) = F(t) - \langle F \rangle$ around the mean intensity $\langle F \rangle$ in a 2D Gaussian detection volume $\exp(-2r^2/r_0^2)$ was calculated. The detection spot size r_0 was 31 lattice units ≈ 25 nm, the size experimentally achievable using the stimulated emission depletion (STED) FCS technique [48]. FCS curves were averaged over nine different positions on the lattice and analyzed using the model

$$G(\tau) = G(0) \frac{1}{1 + (\tau/\tau_D)^\beta}, \quad (6)$$

where the characteristic decay time τ_D is the so-called diffusion time, which is related to the diffusion coefficient and the detection spot size (in case of normal diffusion, $\tau_D = r_0^2/(4D)$), and the exponent is used to describe the deviation of the autocorrelation curve from the normal diffusion model. For $\beta = 1$ expression (6) corresponds to normal diffusion, while for $0 < \beta < 1$ it provides a simple way to describe anomalous subdiffusion in FCS [47].

3. Results

3.1. Phase Diagram of the DMPC/DSPC system based on heat capacity data

The experimentally measured heat capacity curves in figure 3(a) capture the well-known feature of two-component lipid mixtures (see, e.g., [11]), namely, that in a two-lipid system with a fixed composition the all-fluid and all-gel states of the membrane are separated by a temperature range where coexistence of the fluid and gel phases takes

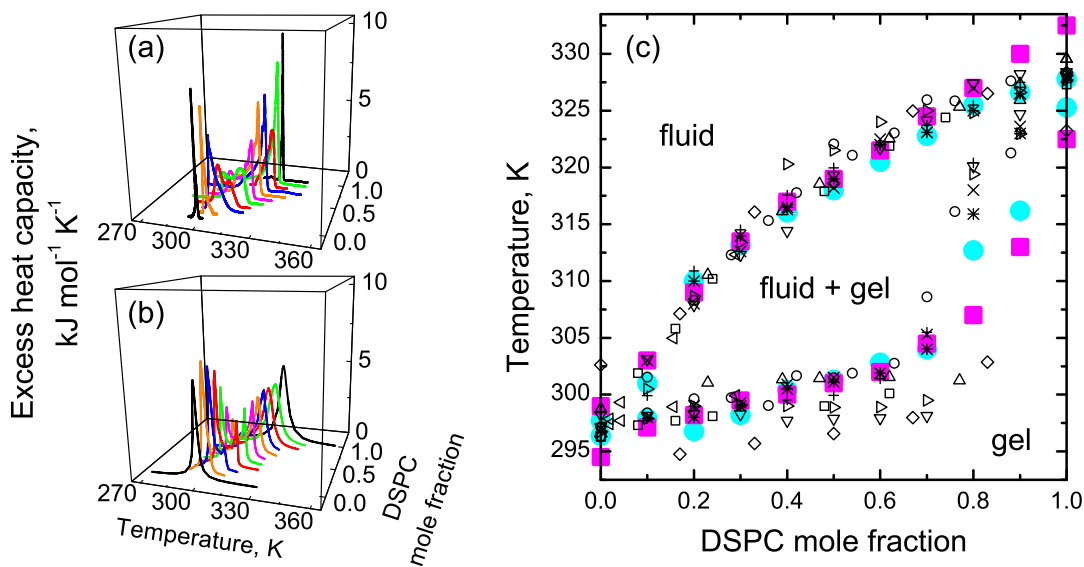


Figure 3. (a, b) Excess heat capacity curves for DMPC/DSPC lipid membranes for a range of compositions (DMPC/DSPC = 0/100, 10/90, 20/80, ..., 90/10, 100/0) measured experimentally by differential scanning calorimetry (a) and obtained in our MC simulations (b). (c) Empirical phase diagram of DMPC/DSPC constructed from the excess heat capacity curves. Experimental data: present work (●), [31] (□), [32] (○), [33] (◇), [34] (▽), [35] (◁), [36] (△), [29] (▷), [30] (×). Monte Carlo simulation data: present work (■), [29] (+), [30] (*).

place. This temperature range can span several tens of degrees. By contrast, phase coexistence is not observed in single-lipid systems, which, upon cooling down below the phase transition temperature, directly undergo a transition from the fluid to gel state.

After successfully adjusting the interaction parameters w_{ij}^{mn} for the simulation of DMPC/DSPC on the square lattice, we find that our MC simulations reproduce well the experimentally measured excess heat capacity curves $C(T)$, as shown in figure 3(a, b).

Historically, in the lipid studies, one usually speaks about broadening of the transition in a two-lipid system (here, by transition, one means the fluid–gel transition, and the broadening is understood as compared to a single-lipid system), and the onset and completion temperatures determined from experimental data are usually discussed, with a fluid–gel phase coexistence region located between these temperatures [29, 31, 35]. Going beyond the empirical experimental approach, one finds that the transition from a single-phase state of the membrane to a two-phase coexistence state is actually a phase transition by itself. A two-lipid system upon cooling from a high temperature at which it is in the fluid state, would thus undergo two phase transitions: from the fluid state to the fluid–gel coexistence, and, upon further cooling, another phase transition from the fluid–gel coexistence to the gel state. To avoid confusion, we clarify that, wherever the expression “phase transition” in the present paper is applied to a two-lipid system, the phase transition from a single phase state into a two-phase coexistence state (or vice

versa) is referred to. Studying the properties of these phase transitions, we believe, can reveal many details on the microscopic organization of the lipid membrane.

Heat capacity curves $C(T)$ (both obtained experimentally and in MC simulations) can be analyzed using the empirical tangent method to determine the onset and completion temperatures (i.e., estimates of the temperature of the transition from a single-phase state to two-phase coexistence), and, as a result, an experimental phase diagram for the binary lipid mixture can be constructed. As is evident from figure 3(c), our MC simulation-based data are in perfect agreement with experimental results (both obtained in the present work and published earlier by other groups [29, 30, 31, 32, 33, 34, 35, 36]), as well as with results from the previous simulation studies [29, 30] carried out on the triangular lattice of lipid chains. This shows that the particular choice of a lattice geometry for lattice-based MC simulations should not be important, provided the lipid interaction parameters are chosen in a proper way.†

It should be pointed out that generally there is neither proof nor guaranty that the onset and completion temperatures extracted from the $C(T)$ curves by the tangent method necessarily correspond to the actual temperatures for the phase transitions from the gel state to fluid–gel coexistence and from fluid–gel coexistence to the fluid state, respectively. Therefore, the *empirical* phase diagram constructed on the basis of heat capacity data may differ from the real phase diagram of the system and thus not provide an insight into the microscopic structure and the dynamics of the membrane.

3.2. Phase separation behaviour of the DMPC/DSPC system. Binodals and spinodals

A closer look at the membrane snapshots from the MC simulation at different compositions and temperatures, as shown in figure 4, indeed reveals that the phase behaviour is, in fact, more complicated. In the region bounded by the curves of the onset and completion temperatures, as determined from the experimental and simulated $C(T)$ data (circles and crosses in figure 4), two types of phase behaviour can be observed: i) complete separation of the gel and fluid phases and ii) a highly dynamic intermixing of the two phases. To gain better understanding of this phenomenon, the radial autocorrelation function $G(r)$ (2) and the structure function $S(k)$ (4) were calculated for a wide range of membrane compositions and broad temperature intervals covering the whole area of the phase diagram. Importantly, our simulations allow us to study $G(r)$ and $S(k)$ for the spatial distributions of both lipids (DMPC or DSPC) and their states (fluid or gel) independently, thereby providing us with valuable details on the microscopic lipid organization in the membrane and its role in the dynamics of the phase separation.

We found that outside the region with a clear coexistence of two phases (the exact boundaries of this region will be discussed in what follows), structure functions of

† While the arguments in favour of representing a lipid membrane as a triangular lattice of lipid chains may seem more or less sound in case of the gel state of the membrane, they do not look nearly as convincing in case of the fluid state.

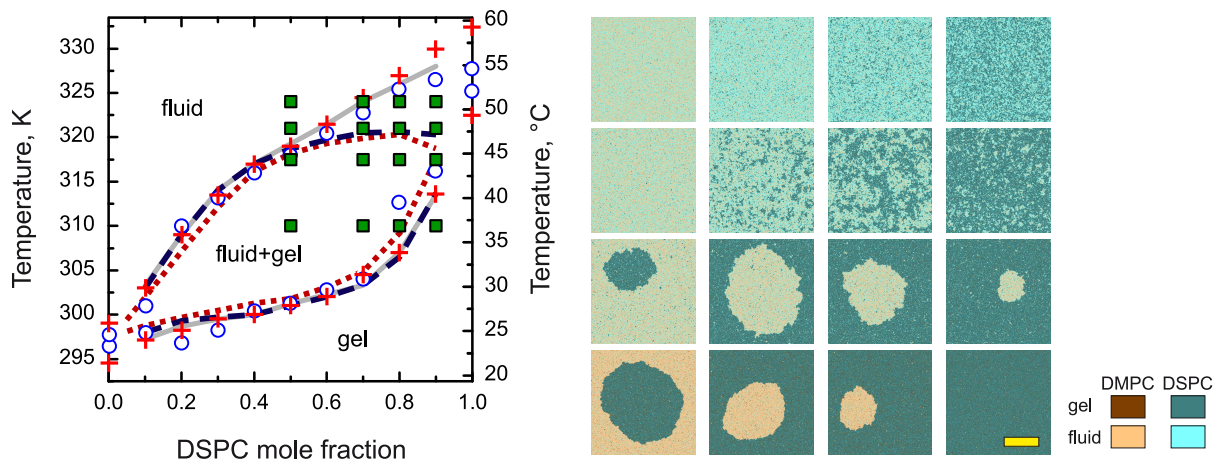


Figure 4. Left-hand panel: Phase diagram of the DMPC/DSPC lipid mixture. Empirical results obtained from the analysis of excess heat capacity curves from differential scanning calorimetry measurements (\circ) and MC simulations ($+$). Lipid state spinodal (---), lipid state binodal (— — —) and lipid demixing curves (—). Filled squares indicate the compositions and temperatures of the equilibrium membrane configurations in the right-hand panel. Lattice size: 600×600 ; scale bar: 200 lattice units \approx 160 nm.

lipid states $S_S(k)$ are well described by the Ornstein–Zernike (OZ) approximation [45] $S_S(k) = S^{OZ}(k) = S_0/[1 + (\xi k)^2]$, where k is a wavenumber, ξ is the correlation length of fluctuations, and the amplitude S_0 is proportional to the order parameter susceptibility of the system.‡

The analysis of the structure functions in terms of the OZ approximation allowed us to study the temperature dependences of the correlation length $\xi_S(T)$ and the amplitude $S_{S,0}(T)$ of the structure function, and thus to determine the lipid state spinodal and binodal. The spinodals were determined by extrapolating the $1/S_{S,0}(T)$ dependence to zero crossing, whereas binodals were determined from the condition $d(1/\xi_S(T))/dT = 0$ [49].

Surprisingly, we found that the phase diagram based on the binodal and spinodal curves differs significantly from the empirical phase diagram obtained from the heat capacity data (figure 4).

What is the reason for such a strong difference? To answer this question, we analyzed the structure functions $S_L(k)$ characterizing the spatial distribution of lipids in the membrane outside the phase coexistence region. Quite unexpectedly, it turned

‡ The order parameter susceptibility characterizes the sensitivity of the order parameter in the system to the external perturbation. For example, for a liquid–gas transition the order parameter is the local density in the system, and the role of the order parameter susceptibility is played by the isothermal compressibility; in case of the Ising model consisting of magnetic spins, one deals, correspondingly, with the magnetic susceptibility. In the membrane system in question, the local order parameter corresponds to the lipid conformation, and the order parameter susceptibility will, among other things, characterize the efficiency of lipid domain formation around proteins preferentially wetted by one of the membrane phases (see [38] and refs. therein).

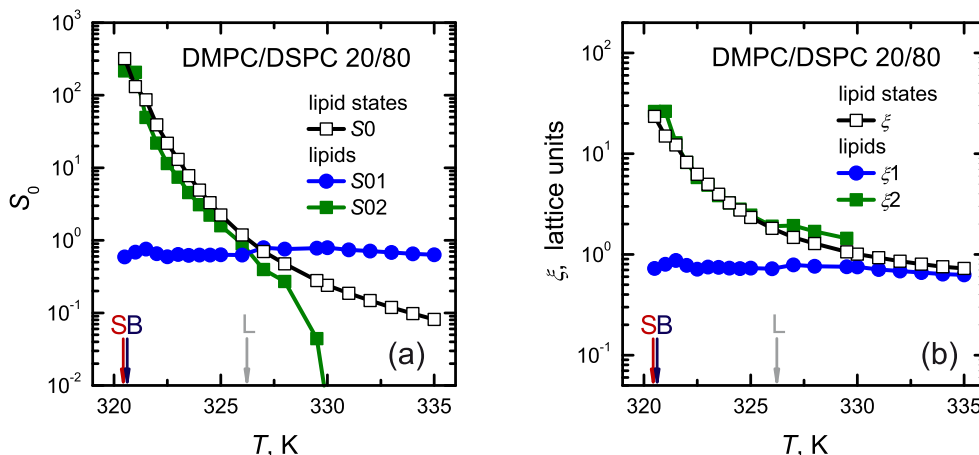


Figure 5. Temperature dependences of the amplitudes (a) and correlation lengths (b) of the OZ components for lipids and lipid states of the DMPC/DSPC 20/80 mixture. The arrows indicate the positions of the binodal (B), spinodal (S), and lipid demixing (L) temperatures.

out that the structure functions of lipids cannot be adequately described by the simple OZ approximation, and two OZ components are necessary to provide an adequate fit of the structure functions of lipids: $S_L(k) = S_{L1}^{OZ}(k) + S_{L2}^{OZ}(k)$.

It should be noted that in order to provide a perfect fit of the $S_S(k)$ and $S_L(k)$ data within the whole range of wavenumbers required that a small positive offset had to be included into the corresponding fit functions. This offset, being important only at high k -numbers, is clearly a consequence of carrying out simulations on a finite-size lattice, and was consistently reproduced in our simulations of the Ising model on the square lattices of the corresponding sizes (data not shown).

It appears that parameters $S_{L1}^{OZ}(0)$ and ξ_{L1} of the first OZ-component only weakly depend on temperature and correspond to demixing of lipids in the same state; $S_{L2}^{OZ}(0)$ and ξ_{L2} , on the other hand, show strong temperature dependences similar to those of $S_S(0)$ and ξ_S (figure 5(a, b)) and thus reflect the appearance of dynamic domains.

We found that for each lipid composition, the temperature at which the amplitudes of the two OZ components used to describe the structure function of the spatial distribution of lipids are equal, $S_{L1}^{OZ}(0) = S_{L2}^{OZ}(0)$, perfectly matches the temperature corresponding to the peak in the $C(T)$ profile. Physically, this means that at this temperature the susceptibilities responsible for the spontaneous clustering of molecules of the same lipid (irrespectively whether they are in the fluid or gel conformation) and their clustering into a particular membrane phase, become equal, and the peak in the heat capacity, in fact, marks the intense local lipid demixing due to transition from a single phase to a two-phase coexistence state. Therefore, we termed the curve defined by the condition $S_{L1}^{OZ}(0) = S_{L2}^{OZ}(0)$ as the *lipid demixing* curve. Notice that the lipid demixing curve very closely approximates the empirical phase diagram based on the heat capacity data (figure 4). Therefore, in what follows we will refer to the boundaries

of the empirical phase diagram as heat capacity-based lipid demixing curves.

We point out that in the region of the phase diagram corresponding to the gap between the binodal and the lipid demixing curve, the membrane shows behaviour characteristic of neither the single-phase nor two-phase coexistence states. Namely, on the one hand, the membrane is not uniform anymore as in the fluid state, while on the other hand, the fluid and gel domains are very poorly defined, have sizes on a wide range of spatial scales, and show non-stop fluctuations without any signs of nucleation and growth.

In fact, this behaviour is characteristic of near-critical fluctuations expected to take place in the vicinity of a critical point. This suggestion is further supported by the behaviour of the binodal and spinodal curves which, within the limits of our accuracy, touch in the corresponding region of the phase diagram, which should take place at the critical point. We will come again to the issue of the critical behaviour of the membrane in more detail later, in sections 3.4 and 3.7.

Here we remark that in an earlier MC simulation-based study of a DMPC/DSPC membrane [50], a conclusion was made based on the analysis of size distributions of fluid and gel clusters, that the phase diagram of this lipid system is much more complicated than that based on heat capacity data (the work [50], however, did not discuss the possibility of the presence of a critical point in the system). Although the quantitative results of the above paper may suffer from a very small system size addressed (40×40 lipid chains), on the qualitative side, these conclusions are largely in agreement with the ones we draw in the present study based on different arguments.

3.3. Transient lipid domains versus thermodynamically equilibrium phases

It has been pointed out elsewhere [11] that, when discussing phase separation in lipid membranes, one should make a clear distinction between the thermodynamically stable phases and (usually, small) transient membrane domains statistically appearing and disappearing in an equilibrated membrane.

In this context, we would like to check to what extent the concept of the thermodynamically equilibrium phase can be applied to results of our simulations. This is important in view of the apparent controversy regarding the application of the lever rule to the phase separation in two-component lipid membranes: on the one hand, the recent laser scanning microscopy experiments on two-component membranes (GUVs) [51] show that the gel and fluid domains in two-component membranes do indeed correspond to thermodynamically equilibrium phases, and therefore the lever rule applies to their description, on the other hand, in previously published MC simulation studies [29, 37] on the DMPC/DSPC systems the authors found out that the fluid and gel phase in the two-phase coexistence region do not follow the lever rule (this was interpreted in [29, 37] as being a consequence of the fact that the gel–fluid transition in DMPC/DSPC mixtures is not a first-order phase transition).

To resolve this contradiction, we studied whether the binodal curves which were

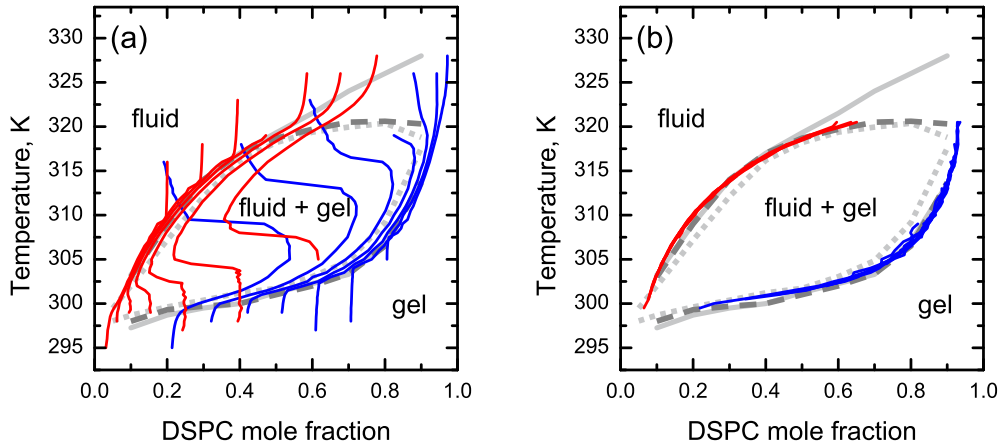


Figure 6. DMPC/DSPC phase diagram reconstructed from the analysis of the temperature-dependent lipid compositions of the fluid and gel phases. Red and blue curves show the compositions (DSPC mole fraction) of the fluid and gel phases, respectively, as a function of temperature for different membrane compositions. (a) Direct calculation from equilibrium membrane configurations. (b) Calculation after selecting the gel and fluid phases by segmentation of the lipid state configurations (see text for details). Additionally, the lipid state binodal (long-dashed curves) and spinodal (short-dashed curves), and lipid demixing curves (grey solid curves) are shown (cf. figure 4).

determined in the previous section of the paper, can be successfully reconstructed by determining for different fixed membrane compositions the temperature dependence of the composition of the individual *phases*, which should exactly be the case if the lever rule applies to the system.

Once one can clearly distinguish between the fluid and gel phases, the problem becomes trivial and is reduced to determining the relative amounts of the two lipids in each of the assigned membrane phases. In practice, of course, this should be carried out using only equilibrium membrane configurations, and averaging over a number of configurations is required to obtain reliable results.

In our analysis, we first assumed, as it has been done in [29], that the fluid and gel phase in a particular membrane configuration are identified with the conformational state of the lipid: all lipids in the fluid conformation are counted as belonging to the fluid phase, and, correspondingly, all lipids in the gel conformation are counted as belonging to the gel phase. The results obtained in this way are presented in figure 6(a). Clearly, this analysis fails to consistently reproduce the binodals of the system, which is in qualitative agreement with previous results of [29].

Our interpretation of the reason why this analysis fails is different from the one previously proposed in [29]. A careful examination of membrane configurations allowed us to conclude that this analysis fails due to the presence of small short-lived fluid or gel domains, which, because of their transient nature, cannot be considered as a part of the thermodynamically stable phase. If counted as belonging to a particular phase,

these domains can severely distort the phase ratio, as well as the lipid composition of the lipid and gel phases, and lead to a break-down of the lever rule.

Therefore, one can hope that, if the small transient membrane domains are excluded from the analysis, and only the thermodynamically stable membrane phases are taken into account, the same analysis will reproduce the binodal curves of the system with a better accuracy.

The problem, thus, boils down to selecting an appropriate rule to discriminate between small transient membrane domains and thermodynamically stable phases. We found that this could be successfully accomplished by low-pass spatial filtering of the lipid state configurations of the membrane. In particular, we found that a procedure consisting of applying a 2D Gaussian filter with the standard deviation of $\sigma = 5$ lattice units and subsequent thresholding the result at the 50% level resulted in consistent reproducible results. § This procedure applied to results of MC simulations with lipid compositions DMPC/DSPC in the range from 20/80 to 80/20, consistently reproduced the upper and lower binodals of the system (figure 6(b)).

The above procedure used for detection of fluid or gel phases in the membrane eliminates from the analysis small domains which contain below ~ 50 lipid molecules, which is in agreement with the intuitive understanding that a portion of a membrane that can be classified into a thermodynamically stable phase should consist of a number of molecules much larger than one. Our present analysis shows that this number is of order of 10^2 . Domains of this size ($\lesssim 10 \times 10 \text{ nm}^2$) are clearly below the optical resolution and are not observable in confocal fluorescence microscopy experiments, which additionally have a finite exposure time, thereby eliminating features fluctuating on a short time scale.

Thus, the apparent controversy between the recent fluorescence microscopy data [51] and previously published results of MC simulations [29] is resolved if one takes into consideration only relatively large and stable membrane domains which constitute the thermodynamically stable phases, which is certainly the case for the domains detectable in fluorescence microscopy experiments.

3.4. Different scenarios of phase transition

A careful examination of the membrane simulation snapshots at various temperatures and lipid compositions shows that, depending on the membrane composition, the phase transition from the fluid phase to the fluid–gel phase coexistence can take place according to two different scenarios.

At compositions for which the lipid state binodal coincides with the lipid demixing curve (see figure 4), the transition has a quasi-abrupt character. This is exemplified in figure 7 by the corresponding temperature sequences of equilibrated membrane snapshots for DMPC/DSPC 80/20 and 50/50. There, lowering the temperature below

§ An approach based on time averaging of membrane configurations over reasonably short simulation intervals was found to give similar results.

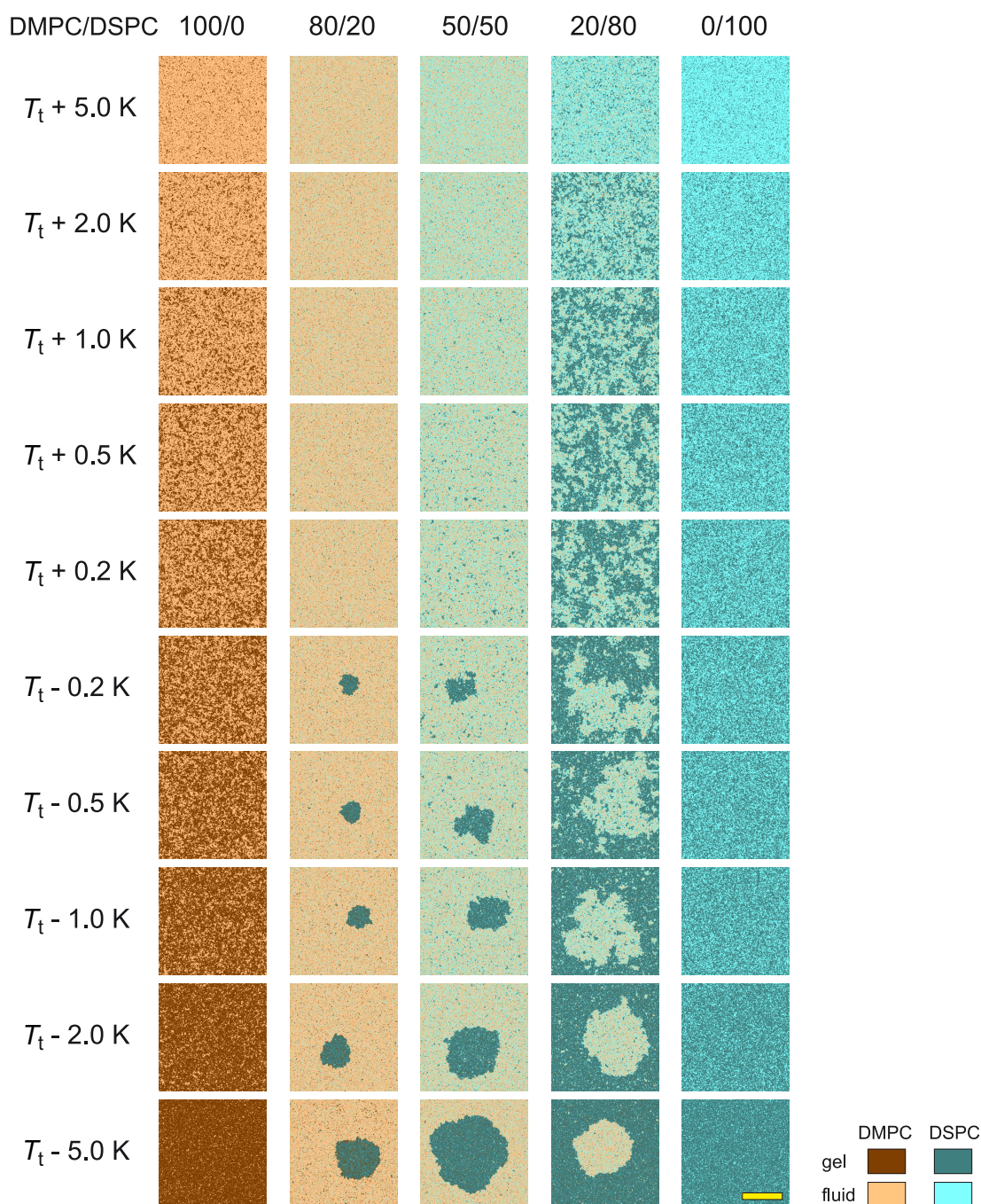


Figure 7. Representative equilibrium configurations obtained in MC simulations of the DMPC/DSPC system with three different compositions DMPC/DSPC = 80/20, 50/50, and 20/80 for a set of temperatures relative to the phase transition from the fluid state to fluid–gel coexistence. For comparison, results for the pure DMPC and DSPC membranes depicting their fluid–gel transitions are shown. Transition temperatures for DMPC/DSPC 100/0, 80/20, 50/50, 20/80 and 0/100 are $T_t = 297.0$ K, 309.7 K, 318.7 K, 320.5 K and 328.0 K, respectively. Lattice size: 400×400 ; scale bar: 150 lattice units ≈ 120 nm. See text for a discussion of the different phase transition scenarios.

the transition temperature T_t immediately leads to an abrupt fluid–gel phase separation and formation of a circular-shaped, stable domain. Above T_t , the membrane stays in all-fluid phase.

On the other hand, in the region of the phase diagram where the lipid demixing curve strongly deviates from the lipid state binodal, a completely different scenario is observed. In particular, when the membrane is cooled down to temperatures below the lipid demixing curve, transient random-shaped fluctuating domains appear. With lowering the temperature, these domains become larger, but remain fractal-shaped and highly dynamic. The mean size of these gel and fluid domains, as well as the order-parameter susceptibility, which are determined from the analysis of the structure function $S_S(k)$, diverge when approaching the temperature of phase transition (see section 3.7). This means that, compared to the scenario discussed above, the character of the transition is changed, and we are dealing with a continuous phase transition. We find that within the corresponding range of lipid compositions, the lipid state spinodal closely approaches the binodal. Eventually these curves touch at a common maximum, i.e. at the point where the compositions of the fluid and gel phase become indistinguishable, which should take place at a critical point. The shapes of the binodal and spinodal curves suggest that the critical composition of the membrane should be close to DMPC/DSPC 20/80. To determine the position of the critical point more exactly, we construct a curve in the phase diagram along which the amounts of lipids in the fluid and gel states are equal: $X_{\text{fluid}} = X_{\text{gel}} = 0.5$. At the critical point one should generally expect that not only the compositions of the fluid and gel phase become indistinguishable, but also their relative contributions become equal.

Indeed, as can be clearly seen from figure 8, this curve crosses the binodal and spinodal lines exactly at the point where they touch, which confirms the presence of a critical point at this position. Thus, in the region of the phase diagram where the lipid demixing curve strongly deviates from the lipid state binodal, approaching the phase transition is accompanied by near-critical fluctuations of the fluid and gel phases. Cooling the membrane to temperatures below the phase transition leads to large-scale phase separation, and a single large domain of a fluid or gel phase is eventually formed in a fully equilibrated membrane. Notice that in the vicinity of the critical point, these domains show strong thermally induced shape fluctuations due to a decrease of the line tension in the vicinity of the critical point (see discussion in section 3.6).

Remarkably, a very similar behaviour was recently observed in experiments on three-component lipid membranes [52]: depending on the membrane composition, the transition to the two-phase coexistence takes place either in an abrupt manner – when the membrane does not pass through a critical point, or via critical fluctuations – when the membrane does pass through a critical point (compare our figure 7 with figure 1(d, e) of [52]).

In addition, we arrive at quite an interesting conclusion: namely, that the binodals of the system are best reproduced via the analysis of the lipid compositions of the fluid and gel phases exactly at those membrane compositions and temperatures where the

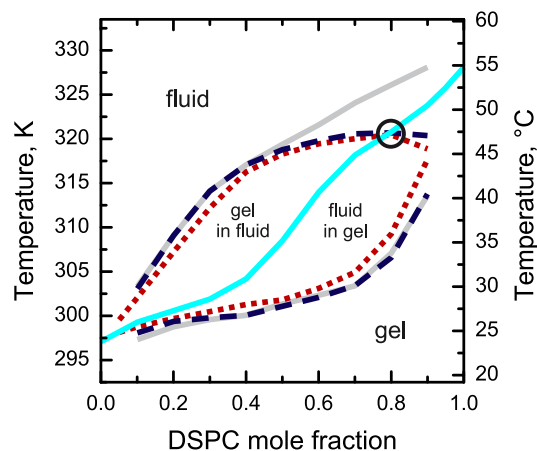


Figure 8. Phase diagram of the DMPC/DSPC system demonstrating the presence of a critical point. Lipid state spinodal (short-dashed lines), lipid state binodal (long-dashed lines) and lipid demixing curves (solid grey lines) are the same as in figure 4. The solid cyan line marks temperatures at which the DMPC/DSPC membrane shows equal amounts of the fluid and gel phase $X_{\text{fluid}} = X_{\text{gel}} = 0.5$. The critical point is marked with an open circle. Within the two-phase fluid–gel coexistence region, areas marked as “gel in fluid” and “fluid in gel” correspond to the gel and fluid minority phases, respectively. Upon complete equilibration, the minority phase always forms a single circular-shaped domain surrounded by the majority phase.

phase transition in the lipid system takes place in a quasi-abrupt manner, i.e., when it is close by its properties to the first-order transition, that is exactly under conditions where this analysis is expected to hold.

In case of a single-lipid membrane, the phase transition also takes place via spatial fluctuations of the fluid and gel domains (see corresponding sequences of membrane snapshots in figure 7). For a single-lipid system, according to the Gibbs’ phase rule, no phase coexistence can take place either above or below the transition temperature. In agreement with that, the results of MC simulations for single lipids in the vicinity of the phase transition show transient fluid or gel domains. Even at the transition temperature the domain sizes are relatively small (~ 100 lipids for DMPC and ~ 20 lipids for DSPC) and, importantly, do not change with an increase of the simulation lattice size. Remarkably, this is in a very good agreement with results of a previous MC simulation study of a DPPC membrane using a ten-state Pink model [53], where the mean cluster size at the transition temperature was estimated to be ~ 40 lipids, in agreement with experimental estimates [54]. Interestingly, this also very well agrees with our estimate of the size of transient lipid clusters we obtained above in section 3.3.

Before concluding this section, three important points should be emphasized.

First, equilibration of the membrane within the fluid–gel phase coexistence region in our simulations always ultimately results in formation of a *single* domain of the minority phase, surrounded by the continuous majority phase. In fact, this should be expected in this system, because in the phase coexistence region of the phase diagram the system

evolution is driven so as to minimize the line tension energy, and, since no explicit or implicit penalties on the domain growth are imposed in the present simulation, a single minority phase domain should eventually be formed. On the other hand, in cases where domains of the minority phase show a different spontaneous curvature compared to the majority phase, the curvature mismatch can result in such a penalty, which at some point stops the growth of domains and prevents their coalescence (see, e.g., [55, 56, 57, 58, 59]). Therefore, the presence of a number of minority phase domains in a two-phase coexistence region in a lattice-based simulation which does not penalize the domain growth and/or coalescence should generally mean that this membrane configuration is still far from the equilibrium one, and therefore, any results on diffusion of lipids (by either studying the time dependence of the mean-square displacement or simulating results of fluorescence correlation spectroscopy (FCS) experiments) obtained in this regime have nothing to do with the equilibrium properties of the membrane.

Second, it is important to emphasize that in our simulations, domains formed in the fluid–gel coexistence region have always circular equilibrium shapes. On the other hand, in some of the previously published lattice-based MC simulation studies, domains quite frequently have a shape of a stripe (see, e.g., [25, 28, 60, 61, 62]), rather than being circular-shaped. We found out that this is a finite-size effect related to the small size of the simulation lattice. We consistently observed similar “stripe-shaped” phase separation in simulations on lattices with a size smaller than $\approx 200 \times 200$ both for our membrane system and the Ising model. For larger lattice sizes, we always find that after equilibration of the system in the phase coexistence region, a single domain with a circular equilibrium shape is formed.||

Third, outside the fluid–gel phase coexistence region, small transient domains can spontaneously form and afterwards spontaneously dissolve after very short time intervals. These domains have a typical diameter of ~ 10 lipids or smaller, and, importantly, their average size does not change with an increase in the size of the simulation lattice. Because of their extremely small size and short lifetime, their presence should be of no importance for optical microscopy-based experiments, as well as for simulations of these experiments at the experimentally relevant spatial scales and time intervals.

3.5. Anomalous diffusion of lipid molecules due to near-critical fluctuations

Diffusion in the lipid membrane is a very important issue, especially in the context of recent experimental observations of anomalous diffusion in cell membranes, the molecular origin of which is still a matter of debate [64, 65, 66]. In case of normal diffusion, the mean-square displacement grows in a linear fashion with time, whereas in case of the anomalous diffusion it is assumed that $MSD(\tau) \sim \tau^\beta$ with $0 < \beta < 1$. This phenomenon is related,

|| Note that the present discussion is restricted exclusively to the finite size effects in the MC simulation studies and is *not* related to experimental findings for two-component membranes, where, depending on the membrane tension, either circular-shaped or stripe-shaped domains can be observed [63].

from a very general point of view, to the presence of dynamic microheterogeneities in the membrane properties, whose existence in cell membranes is explained using the concepts of lipid rafts [2], cytoskeleton-based picket fence [67], and membrane–cytoskeleton interaction [38]. Below we will demonstrate that anomalous diffusion can also take place in freestanding lipid bilayers under conditions of (near-)critical fluctuations.

MC simulations easily give access to trajectories of translational motion of individual lipid molecules, which allows one to obtain time dependence of their mean-square displacement and thus to study the character of diffusion in a most direct way. Experimentally, this corresponds to single-molecule tracking experiments. An alternative way to study diffusion is offered by the fluorescence correlation spectroscopy (FCS) [47]. An FCS experiment can be simulated in a straightforward way based on MC simulation data (for details, see section 2.3.2). One of the advantages of the FCS technique is that it allows to obtain the data on the diffusion of molecules covering many orders of magnitude in time, whereas single-molecule tracking has severe limitations on the single-molecule trajectory length (see, e.g., [68]). The presence of anomalous diffusion is typically associated with a less steep decay of the autocorrelation with time, and the use of the simple expression for the FCS autocorrelation function (6) in the analysis of experimental data can help discriminate the cases of normal ($\beta = 1$) and anomalous ($0 < \beta < 1$) diffusion. The wide time range accessible to FCS measurements along with a relatively simple data analysis explain why the FCS technique is so widespread in experimental studies of the membrane diffusion. ¶

Before presenting our results (which are discussed in more detail in [38]), we would like to discuss the potential situations where one can expect to detect deviations from the normal diffusion in FCS measurements on lipid membranes.

For lipid compositions and temperatures within an area enclosed by binodal curves on the phase diagram, the equilibrated membrane will always show macroscopic phase separation if no penalties on the domain growth and coalescence are imposed. (This is, of course, also true for three-component or multicomponent membranes, except for a much more complex phase diagram in the latter cases.) In an experiment on a free-standing membrane (e.g., giant unilamellar vesicle), this will amount to formation of domains with the sizes of a few micrometers or larger (figure 1). Therefore, from the experimental viewpoint, carrying out FCS measurements in such a membrane should not lead to any unexpected results: since an experimentalist would naturally park the detection spot in a gel- or fluid-phase domain reasonably far from its boundaries, normal diffusion with a diffusion coefficient dependent on the domain phase is expected and indeed experimentally observed [69, 70]. The same principles, obviously, apply to FCS measurements on supported lipid bilayers exhibiting macroscopic phase separation with domain sizes of a few micrometers [71].

In some cases, small, submicrometer-sized domains can be observed in supported bilayers [72, 73, 74]. These small domains do not evolve in size and do not exhibit

¶ This, of course, does not mean that the technique is free from experimental or data analysis artifacts - see, e.g., [47].

translational motion, which indicates that most likely they are pinned to defects on the substrate. Not surprisingly, our standard FCS measurements (the detection spot size was varied from 200 to 260 nm) on supported membranes with the same composition as in [74] did not reveal any signs of anomalous diffusion on such a supported membrane with submicrometer phase separation [75].

In some of the previous studies, FCS measurements were carried out on supported multilayered stacks of lipid bilayers within the phase coexistence region. There, except for perhaps the bilayer immediately adjacent to the solid substrate, macroscopic phase separation should take place, accompanied by domain coarsening and slow diffusional motion of domains (as, e.g., is observed in experiments with double supported bilayers [73]). Therefore, an FCS experiment in this case will report an autocorrelation curve averaged over many (~ 50) independent bilayers, which statistically will be in a different state at the position of the FCS detection spot. As a result, a complex autocorrelation curve is expected with contributions of two different phases, which may additionally be complicated, due to domain motion and edges of some of the domains being close to the detection spot. Therefore, an analysis of these FCS autocorrelation curves using an anomalous diffusion model (as in [30]) can, in fact, be misleading.

Generally, we believe that, when using the FCS technique, deviations from normal diffusion in an equilibrated ‘free’ lipid membrane (i.e., a single bilayer showing no strong interactions with either a support, or membrane proteins, or (artificial) cytoskeleton meshwork) arising due to phase separation, can only be observed in cases where the membrane is dynamically partitioned in a large number of mobile domains with the sizes of order of the FCS detection spot radius. It is then required that these domains either do not coalesce as a result of repulsive interactions (due to local curvature, charge, or other reasons), or are dynamically created and dissolved due to (near-)critical fluctuations.

It is thus clear, based on the above discussion, that the only region in the phase diagram of the DMPC/DSPC mixture, where one can expect deviations from the normal diffusion in a ‘free’ membrane, is the region of near-critical fluctuations.

In agreement with the above discussion, both the mean-square displacement and FCS autocorrelation curve, measured in single-phase regions or separately in the fluid and gel phases in two-phase coexistence region, show normal diffusion (data not shown).

By contrast, the time- and ensemble-averaged mean-square displacement $MSD(\tau)$ for diffusion of DMPC molecules in a DMPC/DSPC 20/80 mixture slightly above the critical temperature, i.e. in the region of near-critical fluctuations, shows transient anomalous diffusion spanning ca. four orders of magnitude in time (figure 9(a)). We believe that this takes place as a result of diffusion of DMPC molecules on the dynamically re-forming fractal network of the fluid phase (for details, see [38]).

In agreement with the subdiffusive behaviour, simulations of a STED FCS [48] experiment with a realistic detection spot radius of 31 lattice units ≈ 25 nm show pronounced deviations of the fluorescence intensity autocorrelation function $G(\tau)$ from the results expected in case of normal diffusion (figure 9(b)). In this case the autocorrelation function $G(\tau)$ is best described by model (6) with the anomalous

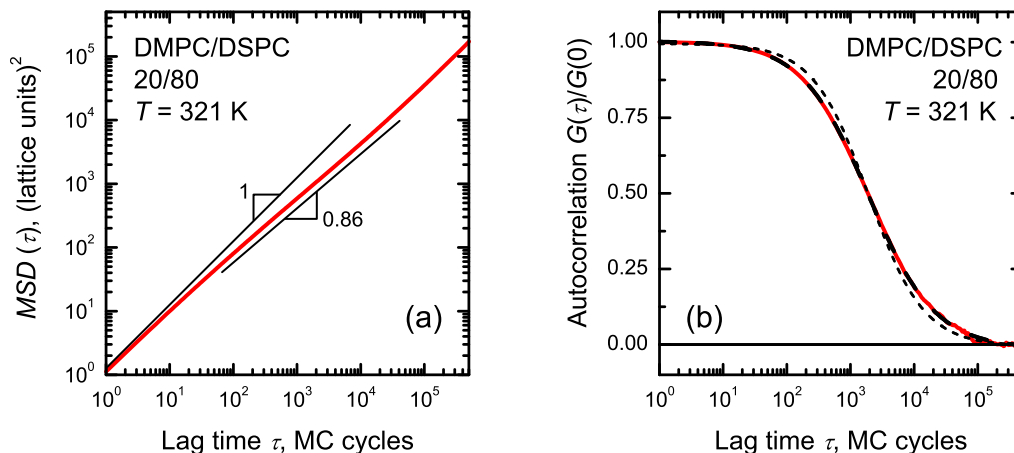


Figure 9. Transient anomalous diffusion of DMPC lipids in a DMPC/DSPC 20/80 membrane at $T = 321$ K, close to the critical temperature. (a) The mean-square displacement $MSD(\tau)$ (red) shows a crossover from normal diffusion at short times to transient anomalous subdiffusion spanning ca. four orders of magnitude in time. (b) The normalized FCS autocorrelation curve $G(\tau)/G(0)$ of a simulated STED FCS experiment (red) along with a fit using the FCS diffusion model (6) (— — —) yielding $\beta = 0.86$. For comparison, a fit with a fixed $\beta = 1.0$ is shown (- - -).

diffusion exponent $\beta = 0.86$.

The FCS results presented in figure 9(b) are obtained in the limit of low concentrations ($< 0.05\%$) of fluorescently labeled lipid molecules, and therefore they reflect the diffusion behaviour of individual lipids. We should point out that FCS curves change quite strongly with increasing the label density in the membrane (data not shown), since fluorescence fluctuations in this case are not only determined by diffusion of individual lipids, but also by their collective motion due to the dynamically reshaping domains. We are planning to address this issue in more details in our future work.

3.6. Line tension

As discussed above, the DMPC/DSPC mixtures at compositions and temperatures corresponding to the fluid–gel phase coexistence region of the phase diagram always display circular-shaped domains, which can be attributed to the presence of an effective line tension between the fluid and the gel phase. After full equilibration the system shows complete phase separation, and only a single domain of the minority phase remains surrounded by the majority phase, which corresponds to minimization of the perimeter of the phase interface, which is driven by minimization of the line tension energy.

These membrane domains show thermally-excited shape fluctuations, as it can be clearly seen in the corresponding membrane snapshots in figures 4, 8, and 10(a–f). An analysis of fluctuating domain shapes should in principle allow one to determine the line tension between the fluid and gel phases in the membrane by analyzing a sequence of fluctuating domain contours. The line tension is then determined from the Fourier

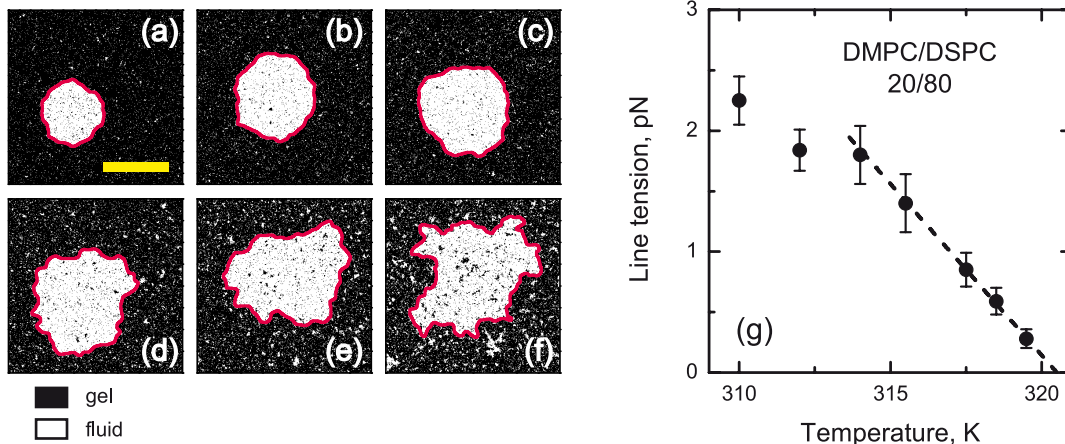


Figure 10. (a-f) Representative equilibrium membrane configurations of DMPC/DSPC 20/80 membrane at $T = 310$ (a), 314 (b), 315.5 (c), 317.5 (d), 318.5 (e), and 319.5 K (f) obtained in MC simulations. The fluid and gel phases are shown as white and black, respectively. Lattice size: 400×400 ; scale bar: 150 lattice units ≈ 120 nm. (g) Line tensions calculated from the Fourier spectrum of domain contour fluctuations (\bullet) and a linear fit of the high-temperature part of these data (---) giving an estimate of the critical temperature $T_c = (320.5 \pm 0.4)$ K.

spectrum of domain contour fluctuations, using the approach originally introduced by Goldstein and Jackson [76] and later successfully applied to lipid bilayer membranes [55, 77] (for corrected expressions, see [78]). One of the important requirements of such an analysis is conservation of the domain area. Unlike the lipid composition of the membrane, which is kept strictly constant during an MC simulation, the relative amount of the gel and fluid phase at a fixed temperature and membrane composition in an equilibrated membrane is conserved only on average. As a result, the domain area is also subject to fluctuations. We have found, however, that the magnitude of these fluctuations is rather low (typically, below 3%), which allows one to consider the domain area as effectively constant and thus to extract the line tension from the analysis of fluctuating domain contours.

To determine the fluctuating contours of a membrane domain, the snapshots of the membrane (reflecting only the conformational state of lipids) were first segmented by applying low-pass filtering (convolution with a 2D Gaussian with $\sigma = 5$ lattice units) followed by thresholding of the result. A set of contours (typically, 200 – 500 contours) was analyzed using a procedure described in [77, 78] to extract the energies of the Fourier modes of domain fluctuations, and ultimately the values of the line tension corresponding to these modes. Since the low-pass filtering procedure employed for domain contour determination suppresses the contributions of the higher-order fluctuation modes, only the first m modes satisfying the condition $m < \pi \langle R \rangle / (6\sigma)$, where $\langle R \rangle$ is the mean domain radius, were used for determination of the line tension. This typically amounted to the line tension analysis based on the first 10 to 20 modes, depending on the domain size.

We found that away from the critical point the line tension of membrane domains obtained from our simulation data is about 2 pN (figure 10(g)). This value is in agreement with experimental values of a few pN reported for membranes with various lipid compositions [55, 58, 62, 77, 78, 79, 80, 81, 82]. Moreover, the line tension of 2 pN is in good agreement with the value expected [81] for the experimentally measured height mismatch of $\sim 0.9 - 1.3$ nm between the gel and fluid phases in DMPC/DSPC membranes [72, 83].

When the membrane temperature and composition approach the critical point, the line tension approaches zero (figure 10), as it is generally expected [84] (see more details below). On the other hand, for lipid compositions displaying a quasi-abrupt phase transition (i.e., compositions with the DSPC fraction of $\sim 50\%$ and below in the high-temperature part of the phase diagram) the line tension does not gradually approach zero as the phase transition temperature is approached (data not shown), which is in agreement with the behaviour illustrated in figure 7.

3.7. Behaviour of the membrane in the vicinity of the critical point

When approaching the critical point, many parameters of a thermodynamic system will either tend to zero or diverge as some power of $|T - T_c|$ [45, 85]. These powers are known as critical exponents.

For example, the correlation length of fluctuations and order parameter susceptibility in a supercritical system diverge upon approaching the critical point with exponents ν and γ , respectively [45]. One therefore should expect that the inverse correlation length and inverse amplitude of the structure function (proportional to the inverse order parameter susceptibility) should vanish close to the phase transition as

$$\xi^{-1}(T) \sim (T/T_c - 1)^\nu \tag{7}$$

and

$$S_0^{-1}(T) \sim (T/T_c - 1)^\gamma. \tag{8}$$

As it is exemplified in figure 11, the inverse correlation length of fluid and gel domains for the DMPC/DSPC 20/80 mixture indeed tends to zero when the system is gradually cooled down to approach the two-phase fluid–gel coexistence region. A linear fit of this dependence yields an estimate of the critical temperature of $T_c = (320.8 \pm 0.1)$ K.

In a similar manner, when approaching a critical point from the two-phase coexistence side, one should generally expect that the line tension vanishes according to the following law [84]:

$$\lambda(T) \sim (1 - T/T_c)^\mu. \tag{9}$$

Indeed, in the case of the DMPC/DSPC 20/80 mixture (figure 10), which is very close to the critical composition, the line tension λ vanishes as the critical temperature T_c is approached and can be well described by a linear dependence $\lambda(T) \sim (1 - T/T_c)$. The linear fit yields $T_c = (320.5 \pm 0.4)$ K.

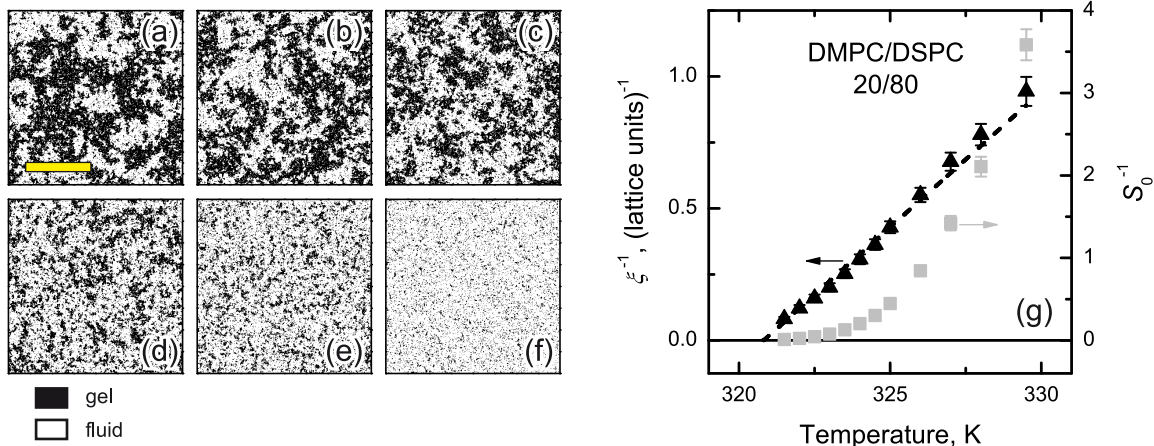


Figure 11. (a-f) Representative equilibrium membrane configurations of the DMPC/DSPC 20/80 lipid mixture at $T = 320.7$ (a), 321.0 (b), 321.5 (c), 322.5 (d), 324.0 (e), and 328.0 K (f) obtained in MC simulations. The fluid and gel phases are shown with white and black, respectively. Lattice size: 400×400 ; scale bar: 150 lattice units ≈ 120 nm. (g) Inverse correlation lengths (\blacktriangle) and inverse amplitude of the structure function (\blacksquare). A linear fit of the temperature dependence of the inverse correlation length (---) gives an estimate of the critical temperature $T_c = (320.8 \pm 0.1)$ K.

These two estimates of the critical temperatures are in good agreement with each other and reproduce well the position of the critical point estimated using the analysis depicted in figure 8.

We can attempt a more precise determination of the critical temperature, as well as the critical exponents of our system by simultaneously fitting the temperature dependences of the inverse correlation length, inverse amplitude of the structure function, and line tension in the vicinity of the critical point to expressions (7), (8) and (9) with a common critical temperature T_c . The results of this fit are shown in figure 12. The estimate of the critical temperature is again close to the above values: $T_c = (320.5 \pm 0.2)$ K. The estimates of the critical exponents obtained in this fit are as follows: $\mu = 1.17 \pm 0.04$, $\nu = 0.97 \pm 0.05$, and $\gamma = 2.94 \pm 0.05$.

It should be noted that different physical systems often show the same set of critical exponents, and in this case are said to belong to the same universality class. This means that close to the phase transition particular microscopic details of a system become unimportant, and its behaviour is governed by a small number of feature, such as dimensionality and symmetry. Recently, it was suggested that three-component membranes close to the critical point might belong to the 2D Ising universality class [52, 62]. For 2D systems in the Ising universality class the critical exponents take the following values [45, 85]: $\mu = 1$, $\nu = 1$, and $\gamma = 7/4$. While the fit in figure 12 gives the estimates of the exponents μ and ν (1.17 ± 0.04 and 0.97 ± 0.05 , respectively) close to those expected for a 2D Ising model, the estimate of the exponent γ (2.94 ± 0.05) absolutely does not fit the predictions for the 2D Ising model.

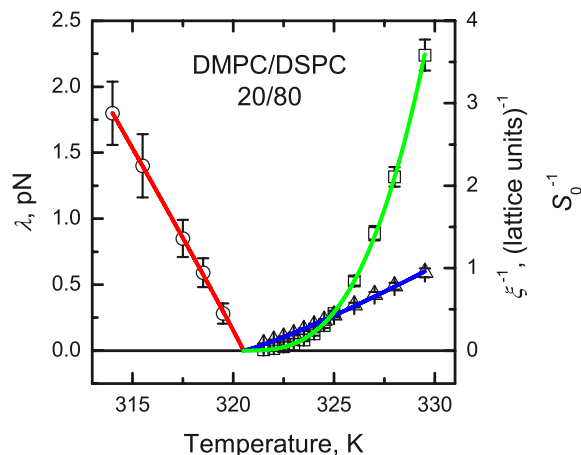


Figure 12. Temperature dependences of the domain line tension $\lambda(T)$ (\circ) below the phase transition temperature, and of the inverse correlation length $\xi^{-1}(T)$ (Δ) and inverse amplitude of the structure functions $S_0^{-1}(T)$ (\square) above the phase transition obtained in MC simulations of the DMPC/DSPC 20/80 lipid system in the vicinity of the critical point. Curves show the global fit of these dependences to the expressions (7), (8) and (9) with a common T_c . The fit yields the estimates of the critical temperature $T_c = (320.5 \pm 0.2)$ K and critical exponents $\mu = 1.17 \pm 0.04$, $\nu = 0.97 \pm 0.05$, and $\gamma = 2.94 \pm 0.05$.

We explain this strong discrepancy of the exponent γ from the Ising model-based expectations by the fact that our system is different from the Ising model in one important aspect. Namely, while the Ising system above the phase transition is characterized by a zero average magnetization (on average equal numbers of up and down spins, or black and white pixels in a graphic representation), our membrane, having an equal amount of lipids in the fluid and gel conformations at the critical point (i.e., having a zero magnetization in terms of the Ising model), very fast transforms into the all-fluid state with increasing the temperature (i.e., in terms of the Ising model, its absolute average magnetization tends to 1). Our preliminary results show that, if, instead of keeping the membrane composition fixed, one would approach the critical point along the curve defined by the condition $X_{\text{fluid}} = X_{\text{gel}} = 0.5$ (cyan curve in figure 8), the exponent γ becomes close to the value of $7/4$ expected for the 2D Ising system.

Thus, based on this behaviour, we conclude that, generally, multicomponent membranes should not necessarily show the Ising criticality.

On the other hand, if the amounts of lipids in the fluid and gel states both stay close to 0.5 within a wide temperature range around a critical point, one can indeed expect to observe critical behaviour close to that of the Ising model. It would be interesting to check experimentally whether this condition holds for three-component model membranes and giant plasma membrane vesicles whose behaviour close to the critical point was recently claimed to follow the Ising criticality [52, 62].

3.8. Domain growth dynamics and dynamic scaling

When the membrane, initially kept at a high temperature, where it is in the all-fluid state, is abruptly cooled down (quenched) to a temperature corresponding to fluid–gel phase coexistence, phase separation takes place, and domains of the gel and fluid phase start to nucleate and coarsen with time. Studying the kinetics of membrane domain growth (coarsening) after a sudden temperature quench into the phase coexistence region can reveal information on the mechanisms involved in phase separation [86] and thus provide further understanding of the microscopic membrane organization and the interplay between the conformational (fluid–gel) state of lipids and their lateral diffusion.

Domain growth in lipid membranes upon a quench to the two-phase coexistence region has been addressed in several experimental works (see, e.g., [73, 81, 87, 88]) and MC simulation studies [28, 60]. We are not aware of any publication where a systematic study of the dependence of the domain growth and dynamic scaling would be carried out for a specific lipid mixture as a function of its composition and/or quench temperature. In this section, we briefly address this issue based on the results of our MC simulations.

After the very early domain growth stage, during which small domains nucleate and become unstable, the stage with the power law growth of the mean size of domains $R(t) \sim t^n$ sets in, with the growth exponent n being characteristic of the system type and growth mechanism [86, 89]. For systems with a non-conserved order parameter $n = 1/2$, whereas for systems with a conserved order parameter the growth exponent can take values of $n = 1/3$ or $n = 1/4$, depending on the particular mechanism of the domain growth. In case where the growth is controlled by evaporation of smaller domains, and larger domains grow due to diffusive transport of material through the medium from domain boundaries with larger curvature to domain boundaries of smaller curvature (Ostwald ripening), one should expect the domain growth with the exponent $n = 1/3$, known as the Lifshitz–Slyozov–Wagner growth [90, 91]. Originally, this law was derived for the growth of minority phase domains in a three-dimensional system in the limit of small minority phase concentration. Later it was argued that the same law also applies to two-dimensional systems, and, based on results of simulations, it was suggested that it should also apply for any concentration of the minority phase [92, 93, 94, 95]. When the domain growth goes via spinodal decomposition, the phase morphology is bicontinuous, and domains initially grow mainly via diffusion along the phase interface, for which $n = 1/4$ [89]. With coarsening of domains, the diffusion through the medium becomes progressively more important and the domain growth crosses over to the asymptotic regime with $n = 1/3$ [96]. On the other hand, if after the quench the phase morphology is not bicontinuous, but rather appears as droplets of the minority phase embedded in the majority phase, the growth proceeds mainly via the Brownian motion and coalescence of these droplets. For this growth mechanism, $n = 1/4$ in 2D [89]. At a later stage, the diffusion of the material through the medium becomes more important, and again a crossover to the asymptotic regime with $n = 1/3$ is observed [96].

To study the growth of domains after an abrupt quench of the membrane being originally in the fluid state to a temperature within the coexistence region of the phase diagram, we calculated the radial autocorrelation function $G(r)$ (2) for a set of times t after the quench and extracted the time-dependent domain size $R(t)$, which was defined as a distance r at which the first zero-crossing of $G(r)$ occurs. As it is exemplified in figure 13, a power-law growth with exponents ranging from $n = 1/4$ to $n = 1/3$ is observed in our simulations, in agreement with the theoretical expectations.

Remarkably, by comparing the domain growth shown in figure 13(b) with the experimental data on domain growth in double supported bilayers [73] we find that our simulations reproduce well the absolute rate of domain growth. In particular, extrapolation of the growth law to the later times shows that it takes of order of 100 s for the domains to grow to an average radius of $\sim 1 \mu\text{m}$, in agreement with experiments [73].

We also studied whether dynamic scaling [97, 98] is observed for domain coarsening in the membrane after a quench, i.e. whether the $G(r)$ corresponding to different time instants t after the quench would collapse onto one master curve if replotted as a function of the reduced radius $r/R(t)$. It turned out that dynamic scaling is observed not in all cases, but only when the total fluid fraction X_{fluid} of the membrane is constant in time. The data presented in figure 13 demonstrate this observation.

Figure 13 (a-d) shows an example for a quench to a point of the phase diagram located deep within the region between the two spinodal curves: the membrane with DMPC/DSPC 50/50 was quenched to $T = 310$ K. The fluid fraction X_{fluid} remains constant during domain coarsening, except for a very short initial growth stage. At the same time, the observed growth exponent crosses over from $n \approx 1/4$ at early times to $n \approx 1/3$ at later times. This suggests that the growth first proceeds via coalescence of domains ($n = 1/4$) and later via bulk diffusion from smaller evaporating domains to larger ones ($n = 1/3$). This behaviour can indeed be observed from the time series of snapshots from the simulation. Dynamic scaling of $G(r)$ is observed for the whole time interval where $X_{\text{fluid}}(t) = \text{const.}$

In figure 13 (e-h) an example for a DMPC/DSPC 20/80 membrane that was quenched to $T = 310$ K is shown. The mean domain size grows as $R(t) \sim t^{1/4}$ for the whole time range that was studied, in agreement with the observed domain growth via the coalescence mechanism. The total fluid fraction in the membrane is nearly constant for up to $t \approx 5 \times 10^4$ MC cycles and the $G(r)$ shows dynamic scaling in this time range. At later times $t \approx (1 - 5) \times 10^5$ MC cycles the fluid fraction changes – most probably due to the rearrangement of lipids between the fluid and gel phases – and no dynamic scaling is observed. Finally, at even later times $t > 10^6$ MC cycles the fluid fraction becomes constant again, and dynamic scaling is again observed.

Figure 13 (i-l) shows the results for domain coarsening in a DMPC/DSPC 70/30 membrane quenched to $T = 302$ K. The mean domain size $R(t)$ shows a behaviour qualitatively similar to the first example of the DMPC/DSPC 50/50 membrane, quenched to $T = 310$ K, and grows with an exponent that crosses over from $n \approx 1/4$ at

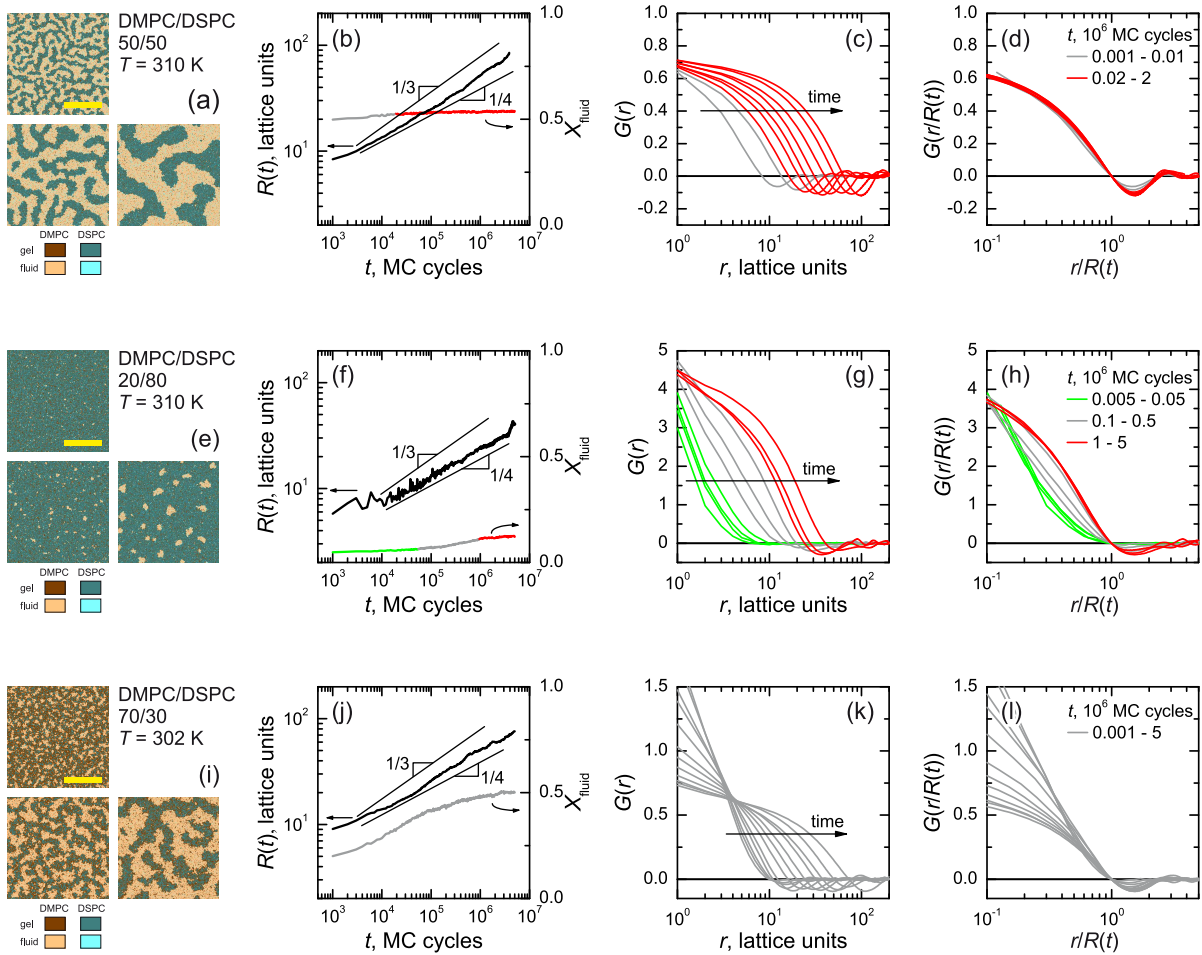


Figure 13. Domain coarsening in DMPC/DSPC 50/50 (a-d), 20/80 (e-h) and 70/30 (i-l) membranes after a sudden temperature quench from $T = \infty$ to $T = 310$ K, 310 K, and 302 K, respectively. Panels (a, e, i) each show three corresponding non-equilibrium configurations of the membrane at times $t = 10^4$, 10^5 , and 10^6 MC cycles after the quench. Lattice size: 400×400 ; scale bar: 150 lattice units \approx 120 nm. (b, f, j) Time dependence of the characteristic domain size $R(t)$ (black curves); thin black lines represent power laws with the exponent of $1/3$ and $1/4$. Also shown are the time dependences of the total fluid fraction $X_{\text{fluid}}(t)$; the time intervals where $X_{\text{fluid}}(t) \approx \text{const}$ are marked by the green and red colours, while the time intervals where $X_{\text{fluid}}(t) \neq \text{const}$ are plotted in grey. (c, g, k) Radial autocorrelation functions $G(r)$ for a set of times (stated in panels (d, h, l)) after the quench. (d, h, l) Same as (c, g, k), respectively, replotted as a function of the reduced distance $r/R(t)$ to demonstrate that dynamic scaling is observed (d, h) when $X_{\text{fluid}}(t) \approx \text{const}$; the colours of the curves at different time instants are chosen to correspond to those of $X_{\text{fluid}}(t)$.

early times to $n \approx 1/3$ at later times, in agreement with the behaviour observed from a time series of membrane snapshots. Nevertheless, no dynamic scaling is observed in this case. Notice that the total fluid fraction under these conditions keeps changing over the whole time interval covered by the MC simulation.

We conclude that this intriguing behaviour reflects a complex interplay between

fluid–gel phase separation and lipid demixing. The equilibration of the total fluid fraction also needs lipid rearrangement via lateral diffusion of lipids, and the timescale of this process depends on the particular point in the phase diagram. This can serve as a potential explanation for the discrepancy in the experimental data on domain growth dynamics in lipid bilayers giving growth exponents from $n \approx 1/3$ [73, 81] down to $n \approx 0.15$ [88] (we should point out here that a careful analysis of the results published in [88] shows that the late-stage growth kinetics exhibits the exponent close to $1/4$, rather than 0.15 reported by the authors). We believe that further insight into these issues can be gained by applying the theory of non-equilibrium phase transitions and ageing [98] and by comparing the outcome of the simulation results with outcomes of appropriately designed experiments.

4. Conclusions

In this paper, we have demonstrated that the properties of lipid membranes on the experimentally relevant spatial scales of order of a micrometer and time ranges of order of a second can be successfully addressed via lattice-based Monte Carlo simulations with very moderate computational efforts.

Using the DMPC/DSPC mixture as an example of a two-component lipid membrane, our large-scale simulations allowed us to obtain the following important results, which, to the best of our knowledge, were previously not reported in simulation studies of lipid membranes:

We found that within a certain range of lipid compositions, the phase transition from the fluid phase to the fluid–gel phase coexistence proceeds via near-critical fluctuations, while for other lipid compositions this phase transition has a quasi-abrupt character. Qualitatively, this is in excellent agreement with recent experiments where these two scenarios of the phase transition were observed in three-component lipid membranes [52].

In the presence of near-critical fluctuations, close to the critical point of the membrane, lipids show transient subdiffusion, which is important for understanding the origins of anomalous diffusion in cell membranes, especially in view of the recent experimental results [52], showing the critical behaviour in giant plasma membrane vesicles isolated from living cells.

In the fluid–gel phase coexistence region, macroscopic phase separation takes place, and after full equilibration of the membrane, a single circular-shaped domain of the minority phase emerges. Analysis of the thermally-induced domain shape fluctuations allowed us to obtain the line tension between the fluid and gel phases. We found that in the fluid–gel coexistence region, away from the critical point, the line tension is ≈ 2 pN, in good agreement with the available literature data on line tension in lipid membranes [55, 58, 62, 77, 79, 80, 81, 82].

When approaching the critical point, the line tension, as well as the inverse correlation length of fluid–gel spatial fluctuations, and the corresponding inverse order

parameter susceptibility of the membrane, approach zero. This is in agreement with recent experimental observations of the approach to criticality in three-component lipid bilayers and giant plasma membrane vesicles [52, 62]. On the other hand, contrary to the conclusions drawn in [52, 62], we find that our system is not in the Ising universality class and provide a tentative explanation for this discrepancy.

An analysis of the domain coarsening dynamics after an abrupt quench of the membrane to the fluid–gel coexistence region revealed that the domain growth law may depend on the lipid composition and temperature, which reflects a complex interplay between fluid–gel phase separation and lipid demixing. We find that the domain growth exponent varies from $1/4$ to $1/3$, which is in a qualitative agreement with experimental data for lipid bilayers, for which a range of growth exponents has been reported as well [73, 81, 88]. We found out that the dynamic scaling of the radial autocorrelation function of the spatial distribution of the lipid state over the membrane during the domain coarsening is observed only when the fluid fraction of the membrane stays constant in time, which again shows the importance of lipid diffusion in the domain coarsening dynamics.

Acknowledgements

The authors acknowledge inspiring discussions with H. Rigneault and C. Favard at the early stage of the project.

The work was supported by the Deutsche Forschungsgemeinschaft via Research Group FOR 877 ‘From Local Constraints to Macroscopic Transport’.

References

- [1] Vereb G, Szöllösi J, Matkó J, Nagy P, Farkas T, Vígh L, Mátyus L, Waldmann T A and Damjanovich S 2003 Dynamic, yet structured: The cell membrane three decades after the Singer–Nicolson model *Proc. Natl. Acad. Sci. USA* **100** 8053–8058
- [2] Simons K and Ikonen E 1997 Functional rafts in cell membranes *Nature* **387** 569–572
- [3] Garg S, Tang J X, Rühle J and Naumann C A 2009 Actin-induced perturbation of PS lipid–cholesterol interaction: A possible mechanism of cytoskeleton-based regulation of membrane organization *J. Struct. Biol.* **168** 11–20
- [4] Liu A P and Fletcher D A 2006 Actin polymerization serves as a membrane domain switch in model lipid bilayers *Biophys. J.* **91** 4064–4070
- [5] Roux A, Cuvelier D, Nassoy P, Prost J, Bassereau P and Goud B 2005 Role of curvature and phase transition in lipid sorting and fission of membrane tubules *EMBO J.* **24** 1537–1545
- [6] Sorre B, Callan-Jones A, Manneville J B, Nassoy P, Joanny J F, Prost J, Goud B and Bassereau P 2009 Curvature-driven lipid sorting needs proximity to a demixing point and is aided by proteins *Proc. Natl. Acad. Sci. USA* **106** 5622–5626
- [7] Pike L J 2006 Rafts defined: A report on the Keystone symposium on lipid rafts and cell function *J. Lipid Res.* **47** 1597–1598
- [8] Weissig V (ed) 2009 *Liposomes: Methods and Protocols, Volume 2: Biological Membrane Models (Methods in Molecular Biology vol 606)* (New York Dordrecht Heidelberg London: Springer)
- [9] Deserno M 2009 Mesoscopic membrane physics: Concepts, simulations, and selected applications *Macromol. Rapid Commun.* **30** 752–771

- [10] Elson E L, Fried E, Dolbow J E and Genin G M 2010 Phase separation in biological membranes: Integration of theory and experiment *Annu. Rev. Biophys.* **39** 207–226
- [11] Heimburg T 2007 *Thermal Biophysics of Membranes* (Weinheim: Wiley–VCH)
- [12] Müller M, Katsov K and Schick M 2006 Biological and synthetic membranes: What can be learned from a coarse-grained description? *Phys. Rep.* **434** 113–176
- [13] Bjelkmar P, Niemelä P S, Vattulainen I and Lindahl E 2009 Conformational changes and slow dynamics through microsecond polarized atomistic molecular simulation of an integral Kv1.2 ion channel *PLoS Comput. Biol.* **5** e1000289
- [14] Niemelä P S, Ollila S, Hyvönen M T, Karttunen M and Vattulainen I 2007 Assessing the nature of lipid raft membranes *PLoS Comput. Biol.* **3** e34
- [15] Pandit S A and Scott H L 2009 Multiscale simulations of heterogeneous model membranes *Biochim. Biophys. Acta* **1788** 136–148
- [16] Yuan H, Huang C, Li J, Lykotraftis G and Zhang S 2010 One-particle-thick, solvent-free, coarse-grained model for biological and biomimetic fluid membranes *Phys. Rev. E* **82** 011905
- [17] Pasqua A, Maibaum L, Oster G, Fletcher D A and Geissler P L 2010 Large-scale simulations of fluctuating biological membranes *J. Chem. Phys.* **132** 154107
- [18] Tumaneng P W, Pandit S A, Zhao G and Scott H L 2010 Lateral organization of complex lipid mixtures from multiscale modeling *J. Chem. Phys.* **132** 065104
- [19] Lowengrub J S, Rätz A and Voigt A 2009 Phase-field modeling of the dynamics of multicomponent vesicles: Spinodal decomposition, coarsening, budding, and fission *Phys. Rev. E* **79** 031926
- [20] Wang X and Du Q 2008 Modelling and simulations of multi-component lipid membranes and open membranes via diffuse interface approaches *J. Math. Biol.* **56** 347–371
- [21] Reigada R, Buceta J, Gómez J, Sagués F and Lindenberg K 2008 Phase separation in three-component lipid membranes: From Monte Carlo simulations to Ginzburg–Landau equations *J. Chem. Phys.* **128** 025102
- [22] Haataja M 2009 Critical dynamics in multicomponent lipid membranes *Phys. Rev. E* **80** 020902(R)
- [23] Fan J, Sammalkorpi M and Haataja M 2010 Formation and regulation of lipid microdomains in cell membranes: Theory, modeling, and speculation *FEBS Lett.* **584** 1678–1684
- [24] Mouritsen O G, Boothroyd A, Harris R, Jan N, Lookman T, MacDonald L, Pink D A and Zuckermann M J 1983 Computer simulation of the main gel–fluid phase transition of lipid bilayers *J. Chem. Phys.* **79** 2027–2041
- [25] Jørgensen K, Sperotto M M, Mouritsen O G, Ipsen J H and Zuckermann M J 1993 Phase equilibria and local structure in binary lipid bilayers *Biochim. Biophys. Acta* **1152** 135–145
- [26] Zhang Z, Sperotto M M, Zuckermann M J and Mouritsen O G 1993 A microscopic model for lipid/protein bilayers with critical mixing *Biochim. Biophys. Acta* **1147** 154–160
- [27] Sugár I P, Biltonen R L and Mitchard N 1994 Monte Carlo simulations of membranes: Phase transition of small unilamellar dipalmitoylphosphatidylcholine vesicles *Methods Enzymol.* **240** 569–593
- [28] Jørgensen K and Mouritsen O G 1995 Phase separation dynamics and lateral organization of two-component lipid membranes *Biophys. J.* **69** 942–954
- [29] Sugár I P, Thompson T E and Biltonen R L 1999 Monte Carlo simulation of two-component bilayers: DMPC/DSPC mixtures *Biophys. J.* **76** 2099–2110
- [30] Hac A E, Seeger H M, Fidorra M and Heimburg T 2005 Diffusion in two-component lipid membranes – a fluorescence correlation spectroscopy and Monte Carlo simulation study *Biophys. J.* **88** 317–333
- [31] Shimshick E J and McConnell H M 1973 Lateral phase separation in phospholipid membranes *Biochemistry* **12** 2351–2360
- [32] Mabrey S and Sturtevant J M 1976 Investigation of phase transitions of lipids and lipid mixtures by high sensitivity differential scanning calorimetry *Proc. Natl. Acad. Sci. USA* **73** 3862–3866
- [33] Lentz B R, Barenholz Y and Thompson T E 1976 Fluorescence depolarization studies of phase transitions and fluidity in phospholipid bilayers. 2. Two-component phosphatidylcholine

- liposomes *Biochemistry* **15** 4529–4537
- [34] van Dijk P W M, Kaper A J, Oonk H A J and de Gier J 1977 Miscibility properties of binary phosphatidylcholine mixtures. A calorimetric study *Biochim. Biophys. Acta* **470** 58–69
- [35] Wilkinson D A and Nagle J F 1979 Dilatometric study of binary mixtures of phosphatidylcholines *Biochemistry* **18** 4244–4249
- [36] Nibu Y, Inoue T and Motoda I 1995 Effect of headgroup type on the miscibility of homologous phospholipids with different acyl chain lengths in hydrated bilayer *Biophys. Chem.* **56** 273–280
- [37] Sugár I P and Biltonen R L 2000 Structure-function relationships in two-component phospholipid bilayers: Monte Carlo simulation approach using a two-state model *Methods Enzymol.* **323** 340–372
- [38] Ehrig J, Petrov E P and Schwille P 2010 Near-critical fluctuations and cytoskeleton-assisted phase separation lead to subdiffusion in cell membranes *Biophys. J.* submitted
- [39] Angelova M I and Dimitrov D S 1986 Liposome electroformation *Faraday Discuss.* **81** 303–311
- [40] Vaz W L C, Clegg R M and Hallmann D 1985 Translational diffusion of lipids in liquid crystalline phase phosphatidylcholine multibilayers. A comparison of experiment with theory *Biochemistry* **24** 781–786
- [41] Matsumoto M and Nishimura T 1998 Mersenne Twister: A 623-dimensionally equidistributed uniform pseudo-random number generator *ACM Trans. Model. Comput. Sim.* **8** 3–30
- [42] Preis T, Virnau P, Paul W and Schneider J J 2009 GPU accelerated Monte Carlo simulation of the 2D and 3D Ising model *J. Comput. Phys.* **228** 4468–4477
- [43] Weigel M 2010 Simulating spin models on GPU *Preprint* arXiv:1006.3865v1
- [44] Hansen J P and McDonald I R 2006 *Theory of Simple Liquids* 3rd ed (London: Academic Press)
- [45] Fisher M E 1964 Correlation functions and the critical region of simple fluids *J. Math. Phys.* **5** 944–962
- [46] Allen M P and Tildesley D J 1991 *Computer Simulations of Liquids* (New York: Oxford University Press)
- [47] Petrov E P and Schwille P 2008 State of the art and novel trends in fluorescence correlation spectroscopy *Standardization and Quality Assurance in Fluorescence Measurements II* (*Springer Series on Fluorescence* vol 6) Resch-Genger U (ed) (Berlin Heidelberg New York: Springer) pp 145–197
- [48] Kastrup L, Blom H, Eggeling C and Hell S W 2005 Fluorescence fluctuation spectroscopy in subdiffraction focal volumes *Phys. Rev. Lett.* **94** 178104
- [49] Strobl G 1997 *The Physics of Polymers* 2nd ed (Berlin Heidelberg New York: Springer)
- [50] Michonova-Alexova E I and Sugár I P 2002 Component and state separation in DMPC/DSPC lipid bilayers: A Monte Carlo simulation study *Biophys. J.* **83** 1820–1833
- [51] Fidorra M, Garcia A, Ipsen J H, Härtel S and Bagatolli L A 2009 Lipid domains in giant unilamellar vesicles and their correspondence with equilibrium thermodynamic phases: A quantitative fluorescence microscopy imaging approach *Biochim. Biophys. Acta* **1788** 2142–2149
- [52] Veatch S L, Cicuta P, Sengupta P, Honerkamp-Smith A, Holowka D and Baird B 2008 Critical fluctuations in plasma membrane vesicles *ACS Chem. Biol.* **3** 287–293
- [53] Cruzeiro-Hansson L and Mouritsen O G 1988 Passive ion permeability of lipid membranes modelled via lipid-domain interfacial area *Biochim. Biophys. Acta* **944** 63–72
- [54] Freire E and Biltonen R 1978 Estimation of molecular averages and equilibrium fluctuations in lipid bilayer systems from the excess heat capacity function *Biochim. Biophys. Acta* **514** 54–68
- [55] Baumgart T, Hess S T and Webb W W 2003 Imaging coexisting fluid domains in biomembrane models coupling curvature and line tension *Nature* **425** 821–824
- [56] Auth T and Gompper G 2009 Budding and vesiculation induced by conical membrane inclusions *Phys. Rev. E* **80** 031901
- [57] Ursell T S, Klug W S and Phillips R 2009 Morphology and interaction between lipid domains *Proc. Natl. Acad. Sci. USA* **106** 13301–13306
- [58] Semrau S, Idema T, Holtzer L, Schmidt T and Storm C 2008 Accurate determination of elastic

- parameters for multicomponent membranes *Phys. Rev. Lett.* **100** 088101
- [59] Idema T, Semrau S, Storm C and Schmidt T 2010 Membrane mediated sorting *Phys. Rev. Lett.* **104** 198102
- [60] Jørgensen K, Klinger A and Biltonen R L 2000 Nonequilibrium lipid domain growth in the gel-fluid two-phase region of a DC₁₆PC – DC₂₂PC lipid mixture investigated by Monte Carlo computer simulation, FT-IR, and fluorescence spectroscopy *J. Phys. Chem. B* **104** 11763–11773
- [61] Seeger H M, Fidorra M and Heimburg T 2005 Domain size and fluctuations at domain interfaces in lipid mixtures *Macromol. Symp.* **219** 85–96
- [62] Honerkamp-Smith A R, Cicuta P, Collins M D, Veatch S L, den Nijs M, Schick M and Keller S L 2008 Line tensions, correlation lengths, and critical exponents in lipid membranes near critical points *Biophys. J.* **95** 236–246
- [63] Li L and Cheng J X 2006 Coexisting stripe- and patch-shaped domains in giant unilamellar vesicles *Biochemistry* **45** 11819–11826
- [64] Saxton M J 2007 A biological interpretation of transient anomalous subdiffusion. I. Qualitative model *Biophys. J.* **92** 1178–1191
- [65] Destainville N, Saulière A and Salomé L 2008 Comment to the article by Michael J. Saxton: A biological interpretation of transient anomalous subdiffusion. I. Qualitative model *Biophys. J.* **95** 3117–3119
- [66] Saxton M J 2008 Response to comment by Destainville et al. *Biophys. J.* **95** 3120–3122
- [67] Fujiwara T, Ritchie K, Murakoshi H, Jacobson K and Kusumi A 2002 Phospholipids undergo hop diffusion in compartmentalized cell membrane *J. Cell Biol.* **157** 1071–1082
- [68] Schmidt T and Schütz G J 2009 Single Molecule Analysis of Biomembranes *Handbook of Single-Molecule Biophysics* Hinterdorfer P and van Oijen A (eds) (Dordrecht Heidelberg London New York: Springer) pp 19–42
- [69] Kahya N, Scherfeld D, Bacia K, Poolman B and Schwille P 2003 Probing lipid mobility of raft-exhibiting model membranes by fluorescence correlation spectroscopy *J. Biol. Chem.* **278** 28109–28115
- [70] Bacia K, Schwille P and Kurzchalia T 2005 Sterol structure determines the separation of phases and the curvature of the liquid-ordered phase in model membranes *Proc. Natl. Acad. Sci. USA* **102** 3272–3277
- [71] Chiantia S, Ries J, Kahya N and Schwille P 2006 Combined AFM and two-focus SFCS study of raft-exhibiting model membranes *ChemPhysChem* **7** 2409–2418
- [72] Giocondi M C and Le Grimellec C 2004 Temperature dependence of the surface topography in dimyristoylphosphatidylcholine/distearoylphosphatidylcholine multibilayers *Biophys. J.* **86** 2218–2230
- [73] Jensen M H, Morris E J and Simonsen A C 2007 Domain shapes, coarsening, and random patterns in ternary membranes *Langmuir* **23** 8135–8141
- [74] Johnston I and Johnston L J 2008 Sphingomyelinase generation of ceramide promotes clustering of nanoscale domains in supported bilayer membranes *Biochim. Biophys. Acta* **1778** 185–197
- [75] Ehrig J 2008 *Diffusion in Artificial Lipid Membranes with Phase Separation: A Study by Dynamic Monte Carlo Simulation and Fluorescence Correlation Spectroscopy* Diploma thesis Technische Universität Dresden
- [76] Goldstein R E and Jackson D P 1994 Domain shape relaxation and the spectrum of thermal fluctuations in Langmuir monolayers *J. Phys. Chem.* **98** 9626–9636
- [77] Esposito C, Tian A, Melamed S, Johnson C, Tee S Y and Baumgart T 2007 Flicker spectroscopy of thermal lipid bilayer domain boundary fluctuations *Biophys. J.* **93** 3169–3181
- [78] Camley B A, Esposito C, Baumgart T and Brown F L H 2010 Lipid bilayer domain fluctuations as a probe of membrane viscosity. *Biophys J* **99** L44–L46
- [79] Baumgart T, Das S, Webb W W and Jenkins J T 2005 Membrane elasticity in giant vesicles with fluid phase coexistence *Biophys. J.* **89** 1067–1080
- [80] Tian A, Johnson C, Wang W and Baumgart T 2007 Line tension at fluid membrane domain

- boundaries measured by micropipette aspiration *Phys. Rev. Lett.* **98** 208102
- [81] García-Sáez A J, Chiantia S and Schwille P 2007 Effect of line tension on the lateral organization of lipid membranes *J. Biol. Chem.* **282** 33537–33544
- [82] Blanchette C D, Lin W C, Orme C A, Ratto T V and Longo M L 2007 Using nucleation rates to determine the interfacial line tension of symmetric and asymmetric lipid bilayer domains *Langmuir* **23** 5875–5877
- [83] Giocondi M C, Pacheco L, Milhiet P E and Le Grimmelc C 2001 Temperature dependence of the topology of supported dimirystoyl-distearoyl phosphatidylcholine bilayers *Ultramicroscopy* **86** 151–157
- [84] Widom B 1965 Surface tension and molecular correlations near the critical point *J. Chem. Phys.* **43** 3892–3897
- [85] Hohenberg P C and Halperin B I 1977 Theory of dynamic critical phenomena *Rev. Mod. Phys.* **49** 435–479
- [86] Bray A J 1994 Theory of phase-ordering kinetics *Adv. Phys.* **43** 357–459
- [87] Hu Y, Meleson K and Israelachvili J 2006 Thermodynamic equilibrium of domains in a two-component Langmuir monolayer *Biophys. J.* **91** 444–453
- [88] Saeki D, Hamada T and Yoshikawa K 2006 Domain-growth kinetics in a cell-sized liposome *J. Phys. Soc. Jpn.* **75** 013602
- [89] Furukawa H 1985 A dynamic scaling assumption for phase-separation *Adv. Phys.* **34** 703–750
- [90] Lifshitz I M and Slyozov V V 1961 The kinetics of precipitation from supersaturated solid solutions *J. Phys. Chem. Solids* **19** 35–50
- [91] Wagner C 1961 Theorie der Alterung von Niederschlägen durch Umlösen (Ostwald-Reifung) *Z. Elektrochem.* **65** 581–591
- [92] Huse D A 1986 Corrections to late-stage behavior in spinodal decomposition: Lifshitz-Slyozov scaling and Monte Carlo simulations *Phys. Rev. B* **34** 7845–7850
- [93] Amar J G, Sullivan F E and Mountain R D 1988 Monte Carlo study of growth in the two-dimensional spin-exchange kinetic Ising model *Phys. Rev. B* **37** 196–208
- [94] Rogers T M, Elder K R and Desai R C 1988 Numerical study of the late stages of spinodal decomposition *Phys. Rev. B* **37** 9638–9649
- [95] Rogers T M and Desai R C 1989 Numerical study of late-stage coarsening for off-critical quenches in the Cahn–Hilliard equation of phase separation *Phys. Rev. B* **39** 11956–11964
- [96] van Gemmert S, Barkema G T and Puri S 2005 Phase separation driven by surface diffusion: A Monte Carlo study *Phys. Rev. E* **72** 046131
- [97] Gunton J, San Miguel M and Sahni P S 1983 The dynamics of first-order phase transitions *Phase Transitions and Critical Phenomena* vol 8 Domb C and Lebowitz J (eds) (New York: Academic Press) pp 267–482
- [98] Henkel M and Pleimling M 2010 *Non-Equilibrium Phase Transitions. Volume 2: Ageing and Dynamical Scaling Far from Equilibrium* (Berlin Heidelberg New York: Springer)